https://doi.org/10.5194/gchron-2023-27
Preprint. Discussion started: 9 January 2024

GEOCHRONOLOGY Discussions Open Access EGU

Local Beryllium-10 production rate for the mid-elevation mountainous regions in Central Europe, deduced from a multi-method study of moraines and lake sediments in the Black Forest

Felix Martin Hofmann[1], Claire Rambeau[2], Lukas Gegg[1], Melanie Schulz[1], Martin Steiner[1], Alexander Fülling[1], Laëtitia Léanni[3], Frank Preusser[1], ASTER Team[3,*]

[1]Institute of Earth and Environmental Sciences, University of Freiburg, Freiburg, 79104, Germany
[2]Laboratoire Image, Ville, Environnement (LIVE UMR 7362), CNRS/Université de Strasbourg/ENGEES, France
[3]Aix-Marseille Université, CNRS, IRD, INRAE, Aix-en-Provence, 13545, France
[*]A full list of authors appears at the end of the paper.

Correspondence to: Felix Martin Hofmann (felix.martin.hofmann@geologie.uni-freiburg.de)

Abstract. Beryllium-10 cosmic-ray (CRE) exposure dating has revolutionised our understanding of glacier fluctuations around the globe. A key prerequisite for the successful application of this dating method is a thorough understanding of local production rates of in-situ accumulated ^{10}Be, usually inferred from independently dated regional reference sites. For the mid-elevation (Variscan) mountain ranges of central Europe, no production rate reference site has been available so far. We fill this gap by determining in-situ ^{10}Be concentrations in large boulders on moraines and by applying radiocarbon and luminescence dating to stratigraphically younger lake sediments in the southern Black Forest, SW Germany. The dating methods yielded concordant results and, based on age-depth modelling with ^{14}C ages, we deduced a local ^{10}Be production rate. The resulting Black Forest (BF) production rate is ~11% lower than both those at the nearest reference site in the Alps and the canonical global ^{10}Be production rate. A stronger weathering and snow cover bias and a higher impact of soil, moss and shrub cover at the stud site likely explain this discrepancy. Due to its internal robustness, we suggest applying the BF production rate in future CRE dating studies in Central Europe and for revising existing age estimates which will have crucial implications for understanding past atmospheric circulation patterns.

1 Introduction

Beryllium-10 cosmic-ray exposure (CRE) dating is an invaluable tool for age determination in the field of glacial (e.g., Hofmann et al., 2024), fluvial (e.g., Schoch-Baumann et al., 2022), coastal (e.g., Dawson et al., 2022), and periglacial (e.g., Amschwand et al., 2021) geomorphology as well as for the dating of mass movements (e.g., Hilger et al., 2018). Calculating CRE ages requires effective ^{10}Be production rates at sampling sites to be determined. CRE age calculators (e.g., Balco et al., 2008) utilise physical models, such as the Lifton-Sato-Dunai (LSD) scaling scheme (Lifton et al., 2014), to extrapolate ^{10}Be production rates at reference sites to sampling sites. The production rate is a key parameter and critically determines the robustness of the ages. At independently dated reference sites (e.g., Claude et al., 2014), geological calibration allows for

https://doi.org/10.5194/gchron-2023-27
Preprint. Discussion started: 9 January 2024

determining the rate of the in-situ accumulation of cosmogenic ^{10}Be in rock surfaces with time (cf., Dunai, 2010). Geological calibration often relies on radiocarbon ages of organic material that was deposited soon after the exposure of the sampled rock surfaces (e.g., Goehring et al., 2012). However, several authors (e.g., Lowe et al., 2019) have questioned the robustness of radiocarbon ages that have previously been used for geological calibration. Thus, applying a robust approach, ideally involving multiple dating methods, to a potential ^{10}Be production rate reference site is the best practice to overcome dating-method-specific issues. If several lines of evidence converge, the resulting production rate will be more reliable than a production rate based on a single geochronological method.

Particularly thanks to joint efforts, such as the CRONUS (Cosmic-Ray prOduced NUclide Systematics)-EU project (Stuart and Dunai, 2009), the number of ^{10}Be production rate reference sites has steadily increased over the last decades (see Martin et al., 2017 for a map of production rate reference sites). In the cosmic-ray exposure program (CREp), a common CRE age calculator, Europe is one of the regions with the most published local ^{10}Be production rates. According to Martin et al. (2017), the majority of the European reference sites are situated at elevations below 500 metres above sea-level (m a.s.l.). The only exceptions are Maol Chean Dearg in Scotland (Borchers et al., 2016) and the Chironico landslide in southern Switzerland (Claude et al., 2014), located at elevations of 521 and 761 m a.s.l., respectively. However, for rock surfaces at higher elevation (e.g., Le Roy et al., 2017), snow shielding during winter affects effective production rates stronger than at lower elevation (cf., Ivy-Ochs et al., 2007). Rates of postdepositional weathering/removal of rock ("erosion" or "rock decay" *sensu* Hall et al. 2012) may differ from the production rate reference sites. Thus, extrapolating ^{10}Be production rates from lower elevation reference sites to sampling locations at higher elevation may induce an unwanted bias in CRE ages. In addition, soil and vegetation cover (trees, shrubs, and moss) may influence effective production rates. To solve these issues, some authors (e.g., Boxleitner et al., 2019) corrected their ages for these factors, whereas others have presented uncorrected ages and have interpreted them as minimum estimates (e.g., Protin et al., 2019). Other authors performed sensitivity tests to assess the effect of these factors on ages (e.g., Hofmann et al., 2022). However, obtaining independent age control is the best strategy to validate proposed correction factors.

The formerly glaciated Variscan mountain ranges of Central Europe comprise the Vosges, the Black Forest, the Harz, the Bavarian/Bohemian Forest, and the Giant Mountains (Ehlers et al., 2011). During the Late Pleistocene, the ice masses in these regions lay in the mostly non-glaciated corridor between the ice sheets over northern Europe and the glacier network of the Alps. As previously discussed (e.g., Hofmann et al., 2020), dating the onset of recession from their Late Pleistocene maximum positions could help to evaluate the hypothesis that the Alps shielded the ice caps and glaciers from humid air masses from the Mediterranean Sea when several piedmont glaciers of the Alps reached their last maximum extent (at around 25 ka; e.g., Gaar et al., 2019). Starting with a pioneering study in the Vosges (Mercier et al., 1999), France, CRE dating became the key method for age determination of ice-marginal positions (e.g., Mercier et al., 2000; Reuther, 2007; Mentlík et al., 2013; see Hofmann et al., 2022 for a compilation), allowing for overcoming three major limitations. First, the

https://doi.org/10.5194/gchron-2023-27
Preprint. Discussion started: 9 January 2024

lack of organic material prevented radiocarbon dating of moraines. Second, luminescence and radiocarbon dating of deposits present in cirque basins only gave minimum deglaciation ages (e.g., Vočadlová et al., 2015). Third, although investigating the sedimentary sequence in the overdeepened Elbe Valley in the Giant Mountains (Czechia) undoubtedly provided valuable insights into the environmental history, applying luminescence and radiocarbon dating to sediments below and above the till of the last glaciation only resulted in a bracketing age for the last glaciation. Obtaining a ^{10}Be production rate would offer the opportunity to refine our knowledge of past atmospheric circulation patterns over Europe during the Late Pleistocene.

In this paper, we present a new ^{10}Be production rate reference site in the southern Black Forest, SW Germany (Fig. 1). We chose the Feldsee Cirque (8.0 °E, 47.9 °N WGS 1984 coordinate reference system), since (i) we observed multiple large, quartz-bearing boulders on two moraines and as (ii) a bog, the Feldsee Bog, is situated in the tongue basin of the former glacier whose sediments are stratigraphically younger than those of the moraines (Lang, 2005; Hofmann and Konold, 2023). We first measured the concentration of in situ accumulated cosmogenic ^{10}Be in rock samples from moraine boulders. Obtaining sediment cores from a locality on a buried moraine, applying radiocarbon dating to macrofossils, and age-depth modelling allowed us to determine a minimum age for the moraines. In addition, we applied luminescence dating to the sediment cores to cross-check the results. Based on the ^{10}Be concentrations in rock samples from the moraine boulders and the modelled basal age of the bog sediments, we deduced a local ^{10}Be production rate, hereinafter termed the Black Forest (BF) production rate. Calibrating the local production rate finally offered the opportunity to evaluate the correction factors used by previous authors to correct their CRE ages for the Variscan mountain ranges.

2 Regional setting

2.1 Study area

The study site comprises the Feldsee Cirque with an impressive, up to 300 m high headwall (Fig. 2; LGRB, 2023), and the immediate surrounding area. It is situated east of Feldberg (1493 m a.s.l.), the highest summit of the Black Forest. Lake Feldsee, an up to 33 m deep, moraine-dammed lake, covers the tongue basin on the cirque floor (Wimmenauer et al., 1990). An about 0.03 km^2 large bog, the Feldsee Bog (LUBW, 2006), is located downstream from the ice-marginal moraine at the eastern shore of the lake (Fig. 2). The Feldsee Cirque leads into the Seebach Valley, a well-developed trough valley (Metz, 1985). The Seebach is the main stream in the study area, and originates from above the headwall of the Feldsee Cirque and pertains to the Rhine drainage network (LUBW, 2022a).

The study site belongs to the crystalline (southern) part of the Black Forest that represents the basement of the Variscan orogeny (380-290 Ma; Geyer and Gwinner, 2011). With the denudation of the orogen, various sediments were deposited on top of the Variscan basement under terrestrial and marine conditions during the Permian, Triassic, and Jurassic (Geyer and Gwinner, 2011). Tectonic activity associated with the formation of the Upper Rhine Graben (starting at around 50 Ma;

https://doi.org/10.5194/gchron-2023-27
Preprint. Discussion started: 9 January 2024

Ziegler, 1992) led to uplift of the southern Black Forest and removal of the Mesozoic sedimentary rock. Migmatites, flaser gneisses, and gneisses of the Variscan basement dominate the study area (LGRB, 2013). The uppermost part of the western headwall of the cirque consists of quartz-rich porphyry (LGRB, 2023).

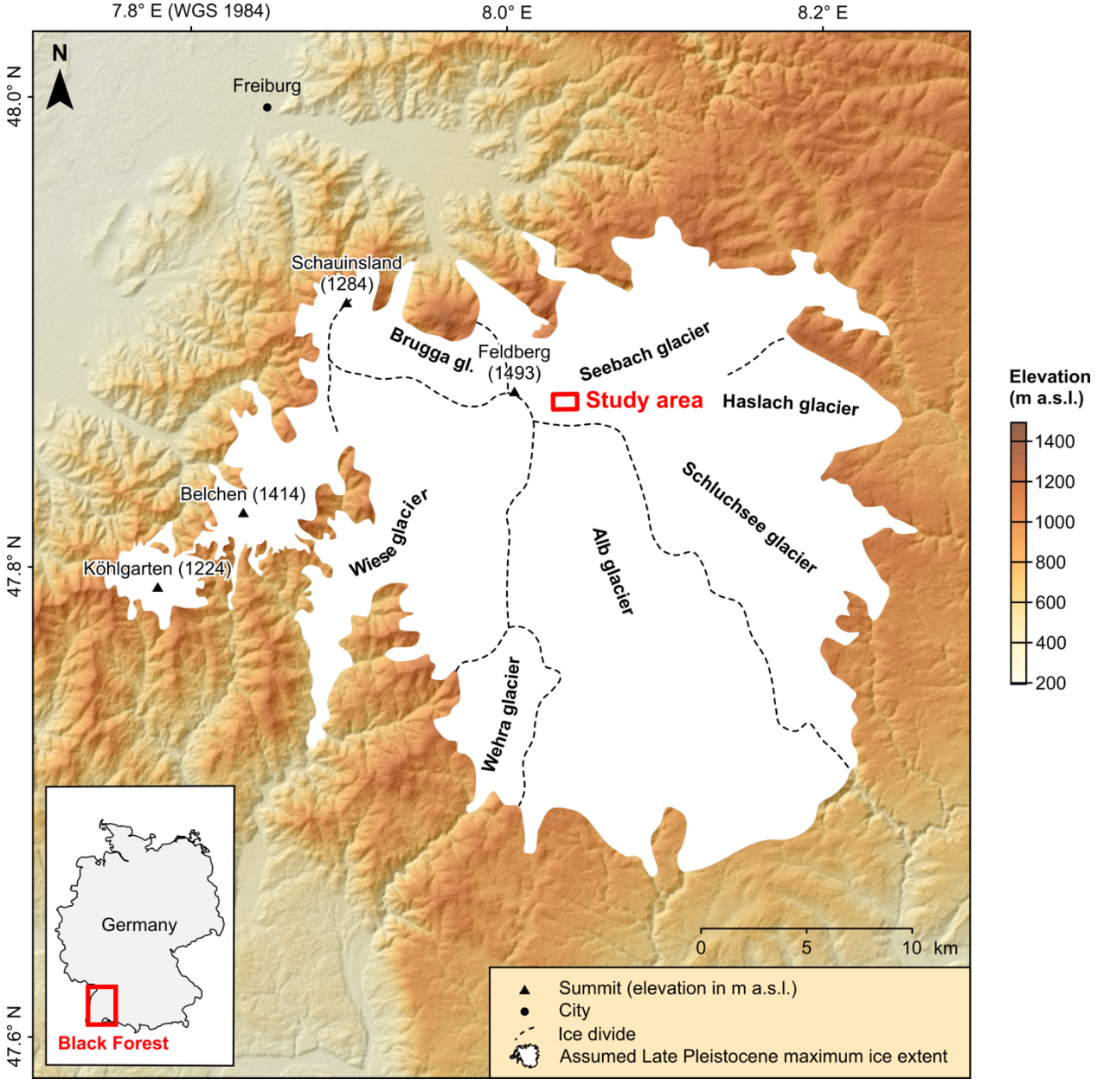

Figure 1: Location of the study area and the assumed Late Pleistocene maximum ice extent in the southern Black Forest (Hemmerle et al., 2016).

https://doi.org/10.5194/gchron-2023-27
Preprint. Discussion started: 9 January 2024

During the Quaternary, the southern Black Forest was repeatedly glaciated. For the last (Late Pleistocene) glaciation, previous reconstructions have pointed towards the existence of four interconnected ice caps, covering an area of about 1000 km² (Metz and Saurer, 2012). The ice cap on Feldberg and the surrounding region was the largest of these ice caps. During the last deglaciation, the ice caps disintegrated into valley glaciers and finally into isolated cirque glaciers (Metz and Saurer, 2012; Hemmerle et al., 2016; Hofmann et al., 2020, 2022, 2023; Hofmann, 2023). However, successive phases of ice-marginal stability punctuated the overall trend of glacier recession. According to ^{10}Be CRE ages for the Sankt Wilhelmer Valley and the Zastler Valley, two valleys north-west of Feldberg, repeated phases of moraine formation occurred no later than 17–16 ka, 14 ka, and by 13 ka at the latest, respectively (Hofmann et al., 2022, 2023; Hofmann, 2023).

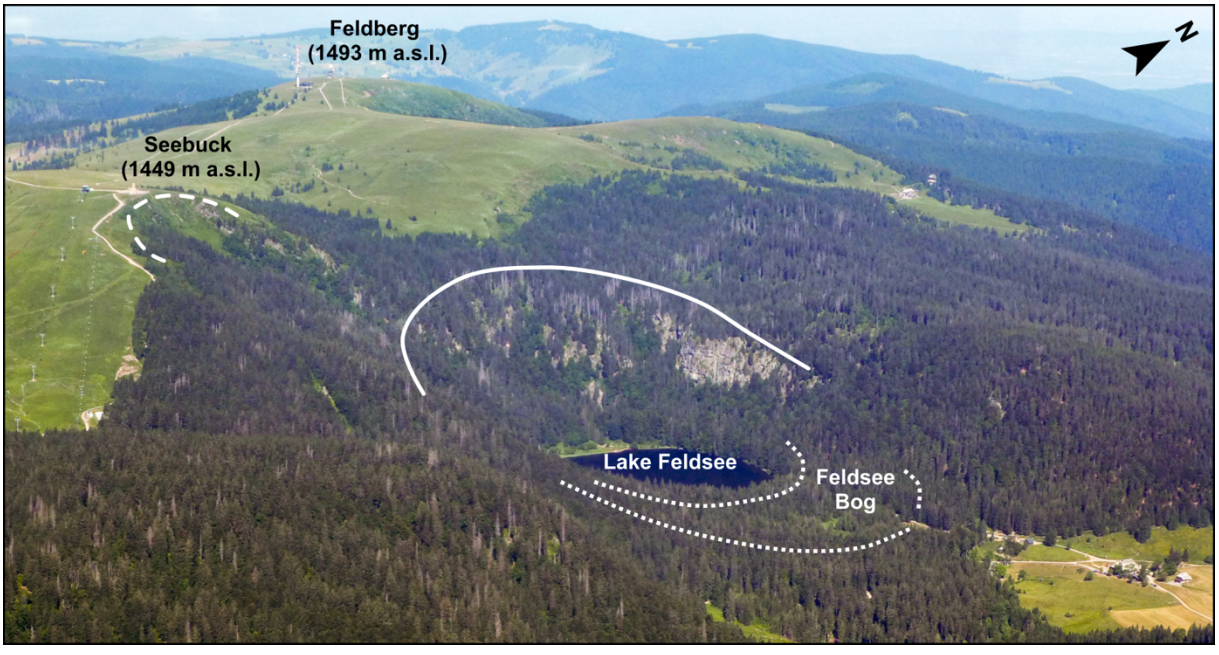

Figure 2: Photo of the study site taken from a glider (photo: Matthias Geyer). It consists of the Feldsee Cirque (marked with a solid white line) with an impressive headwall, and the immediate surroundings. Lake Feldsee, a moraine-dammed lake, covers the tongue basin on the cirque floor. The prominent moraine that delimits the lake to the east is marked with a dotted line. The Feldsee Bog that developed from a former proglacial lake is situated further east. A semi-circular moraine surrounds the bog. Also note the initial cirque (dashed white line) on the north-eastern flank of Seebuck.

According to data of the German Weather Service (DWD), mean annual precipitation and average annual temperature between 1961 and 1990 CE at the weather station on Feldberg (at 1486 m a.s.l.), situated about 1.5 km to the west of the study site, amounted to 1909 mm and 3.3 °C, respectively (DWD, 2023). Snowfall accounted for about two thirds of annual precipitation during this period (Matzarakis, 2012).

https://doi.org/10.5194/gchron-2023-27
Preprint. Discussion started: 9 January 2024

2.2 Previous work

The prominent traces of glaciations in the study area have attracted researchers for more than 150 years. Both Walchner (1846) and Ramsay (1862) already recognised that glaciers shaped the Feldsee Cirque and first described the prominent ice-marginal moraines east of Lake Feldsee. The Feldsee ice-marginal position, named after these prominent ice-marginal landforms, later became a key element for the subdivision of the last deglaciation of the southern Black Forest (Steinmann, 1902; Schrepfer, 1925; Erb, 1948; Liehl, 1982; Metz and Saurer, 2012; Hofmann et al., 2020). Hofmann and Konold (2023) recently revisited glacial landforms at the study site and performed geomorphological mapping at the 1:5000 scale with the aid of a digital elevation model (DEM) derived from light detection and ranging (LiDAR) data (x–y resolution: 1 m; vertical accuracy: ±0.2 m; LGL, 2015) and field evidence. As this is the most recent study on glacial landforms in the study area, we summarise the findings in the following paragraphs (see Fig. 3). As only the ice-marginal moraines of the former Feldsee cirque glacier are relevant for the geological calibration of the local ^{10}Be production rate, we only discuss ice-marginal positions of this glacier but not those (positions SH-01, SH-02, SH-03, SH-04, and SH-05) of a transfluent glacier that advanced from a south-westerly direction into the Seebach Valley (Meinig, 1980).

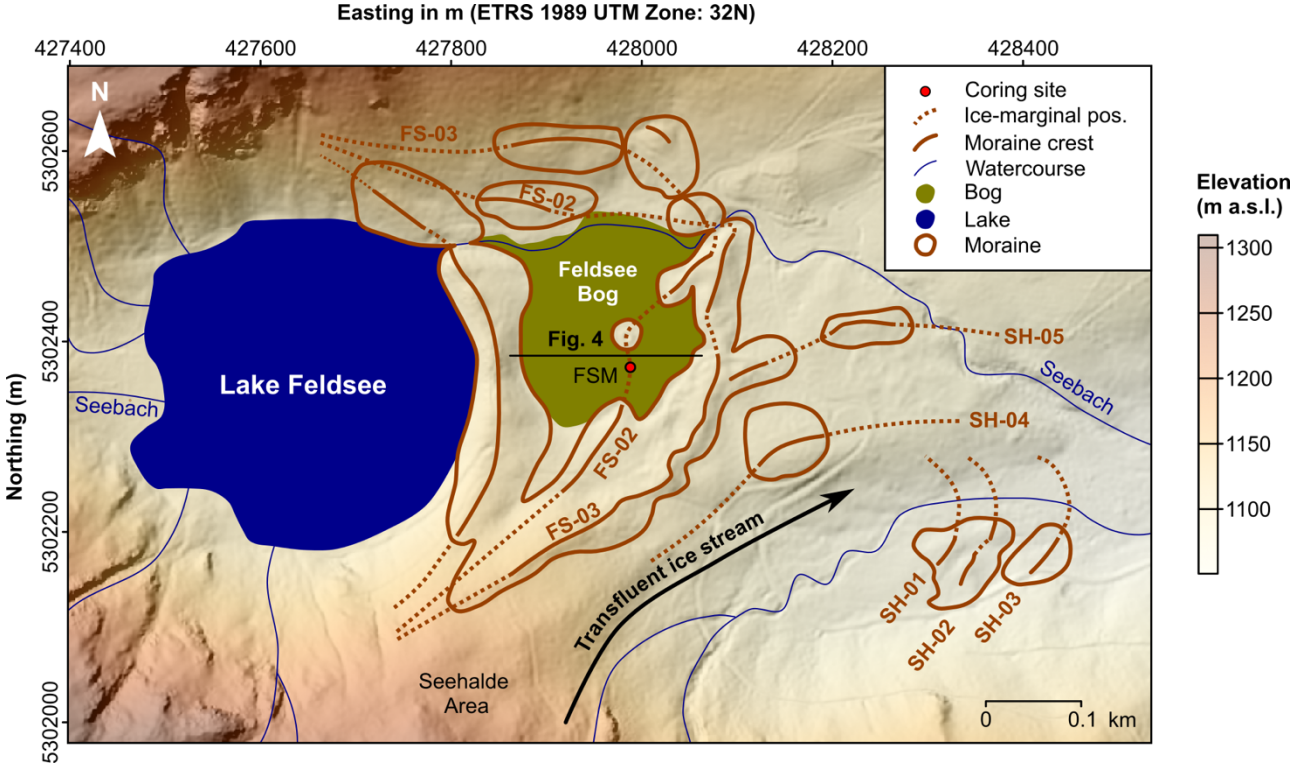

Figure 3: Map of moraines and ice-marginal positions in the study area (Hofmann and Konold, 2023) and the location of the coring site. For the DEM in the background, see LGL (2015).

https://doi.org/10.5194/gchron-2023-27
Preprint. Discussion started: 9 January 2024

The ice-marginal moraines of the Feldsee cirque glacier reflect three positions, named, from the oldest to the youngest, FS-03, FS-02, and FS-01 (Fig. 3; Hofmann and Konold, 2023). A semi-circular and boulder-rich moraine with a sharp crest is located at position FS-03. This moraine partly overlies a moraine at position SH-05. Based on the SW-NE orientation of the latter, this moraine probably formed at the margin of a transfluent ice stream that advanced from the south, i.e., from the Seehalde Area, in a north-easterly direction into the Seebach Valley. As the moraine at position FS-03 overlies those at position SH-05, the semi-circular moraine at position FS-03 must have formed during a re-advance of the Feldsee cirque glacier. The moraine at position FS-02 subdivides the bog in two parts. Peat and lake sediments partly cover the moraine and, therefore, it is only visible south of the bog, in the centre of the bog (Lang, 2005), and at the north-eastern end of the bog. The semi-circular and sharp-crested moraine at position FS-01 dams up Lake Feldsee. According to Schreiner (1990), this landform is one of the morphologically most distinct and best-preserved moraines in the entire southern Black Forest.

In the 1970s and 1980s, Lang et al. (1984) obtained sediment cores at thirteen and five sites from the southern portion of the Feldsee Bog (along a W-E transect; Fig. 4) and Lake Feldsee, respectively (summarised by Lang, 2005). This research revealed the presence of the buried ice-marginal moraine at position FS-02. Lang (2005) proposed that this landform subdivides the Feldsee Bog into two distinct basins. The succession of till, gyttja, clayey gyttja/clay, gyttja, and peat at coring site 5 (Fig. 4) indicated that a proglacial lake formed in the area presently occupied by the bog immediately after deglaciation and that the lake later evolved into a bog (Lang, 2005).

At coring site 5, Lang et al. (1984) observed a thin greyish layer (Fig. 4) that they interpreted as the Laacher See Tephra (dendrochronologically dated to 13006±9 cal. a BP; Reinig et al., 2021). Note that these authors did not properly document the mineralogical characteristics of the apparent tephra which would have more convincingly supported the presence of this precisely dated tephra at the study site. Lang et al. (1984) inferred from the succession of lithostratigraphic units and the position of the apparent tephra at coring site 5 that sedimentation began during the short-lived cooling episode at around 14 ka, often referred to as Older Dryas (cf., Heiri et al., 2014). A light-grey layer was also identified in the sediments of Lake Feldsee and classified as Laacher See Tephra (cf. Lang, 2005). As discussed by Lang (2005), both sites must have been ice-free no later than 13.1 ka.

3 Methods

3.1 Coring

Sediment cores from the Feldsee Bog were obtained during fieldwork in 2021 CE with the aid of a COBRA vibracorer that allowed for extracting sediment cores with a diameter of 5 cm and a length of 1 m. To prevent daylight exposure of the sediments in the cores, the drilling system was equipped with opaque plastic tubes to store individual sediment cores. The

https://doi.org/10.5194/gchron-2023-27
Preprint. Discussion started: 9 January 2024

cores were hydraulically extracted, sealed, and opened in the lab with a circular saw in red-light conditions. Subsequently, loss-on-ignition (LOI) analyses (cf. Heiri et al., 2001) were performed to determine the content of organic matter.

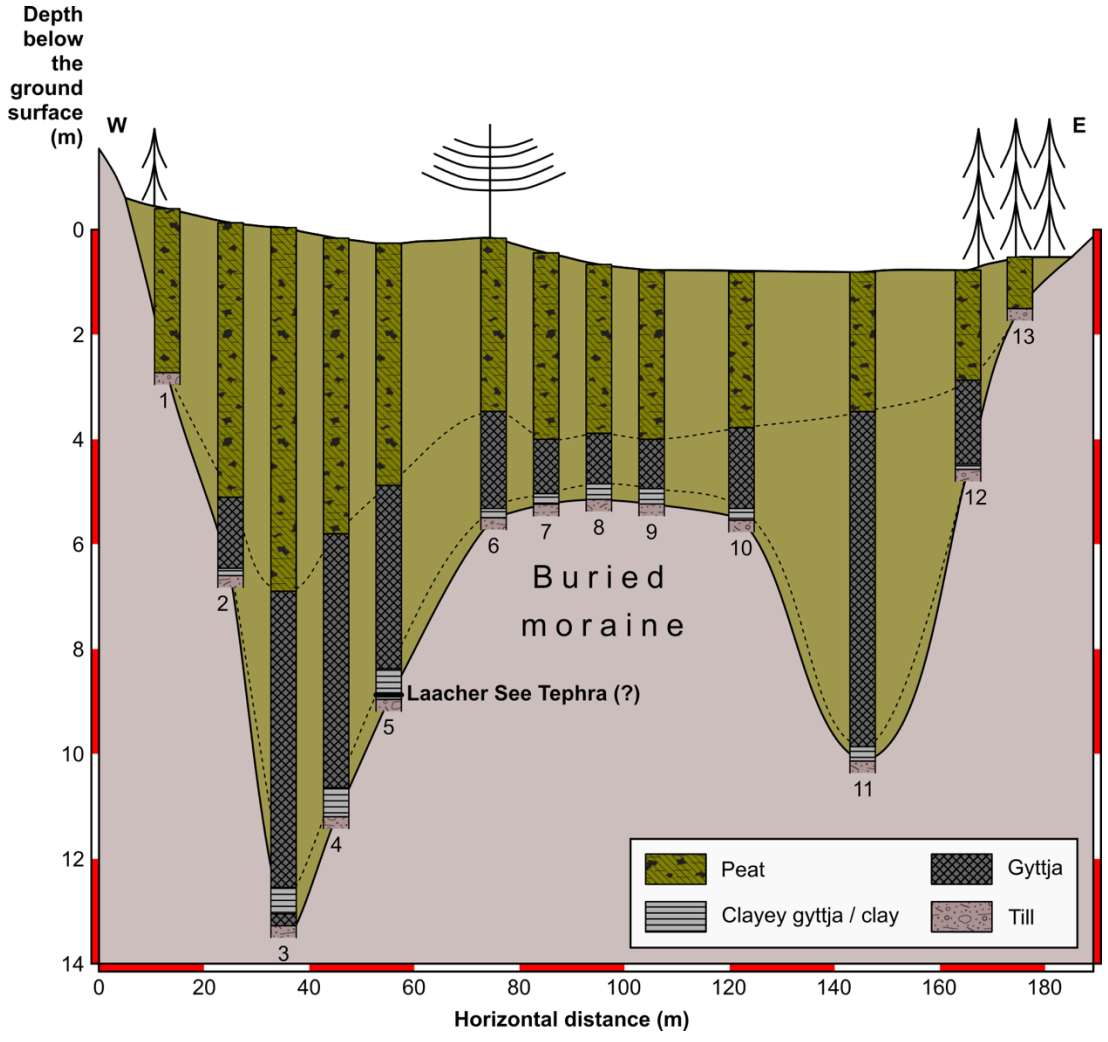

Figure 4: Sedimentary successions at 13 coring sites along a W-E transect in the southern part of the Feldsee Bog. Note the presence of a buried moraine that separates the bog into a deeper western and a shallower eastern basin. The numbers below the cores stand for the coring sites. See Fig. 3 for the location. Redrawn from Lang (2005).

During opening of the cores in the lab, we noted that all sediment cores were shorter than the penetrated depth and, thus, core shortening must have occurred during the coring campaign. Generally, core shortening is one of the main limitations in vibracoring (cf., Glew et al., 2001). As sediments with a higher water content are generally more prone to compaction (cf., Glew et al., 2001), we assumed that only the clayey and silty lake sediments in the cores (water content: 18-85%) were affected by shortening and not the stratigraphically older diamicts (water content: 15-17%). Following Glew et al. (2001), we assumed that the sediments in the cores were progressively thinned down-core, i.e., equally affected by compaction.

https://doi.org/10.5194/gchron-2023-27
Preprint. Discussion started: 9 January 2024

Individual conversion factors were computed for every one-metre-long sediment core which then allowed for adjusting the thickness of the lithostratigraphic units to the penetrated depth.

3.2 Radiocarbon dating and age-depth modelling

Macrofossils (see the supplement for photos of the sampled macrofossils) were hand-picked after core surface cleaning and KOH pre-treatment of bulk samples. A total of nine samples was sent to the radiocarbon laboratory in Poznan, Poland (Table 1) to obtain accelerator mass spectrometry (AMS) radiocarbon ages.

The ^{14}C ages were calibrated with the OxCal software (version 4.4; Bronk Ramsey, 2009) available at https://c14.arch.ox.ac.uk/oxcal/OxCal.html (last access: 18 September 2023), and the IntCal20 calibration curve (Reimer et al., 2020). Age-depth modelling with the online Oxcal program and IntCal20 (Reimer et al., 2020) was undertaken with the aid of ^{14}C ages of macrofossils. The *P_Sequence* function was selected for age-depth modelling, as the sampled macrofossils were assumed to be in correct stratigraphical order and since this function allowed for changes in the sedimentation rate (Bronk Ramsey, 2008). Following the guidelines of Bronk Ramsey and Lee (2013), the model was tuned to find the most suitable value for the *k*-factor, i.e., the number of increments per depth unit. See the supplement for the input-code for the *P_Sequence*.

Table 1: Macrofossils sampled from the sediment cores from the Feldsee Bog.

Sample	Decompacted depth (m)	Laboratory code	Material sampled
FSM-450a	4.28	Poz-153523	Unidentified plant fragment
FSM-450b	4.28	Poz-153524	Unidentified plant fragment
FSM-536	5.24	Poz-151913	Unidentified plant fibre
FSM-538	5.26	Poz-152546	Sphagnum moss
FSM-550	5.43	Poz-152548	Leaf fragments
FSM-553	5.47	Poz-152549	Sphagnum moss
FSM-558	5.54	Poz-152550	Unidentified plant fragment
FSM-560	5.56	Poz-152552	Unidentified plant fragment
FSM-563	5.61	Poz-152419	Unidentified plant fragment

3.3 Luminescence dating

To cross-check the radiocarbon ages, the sediment cores were sampled for luminescence dating. Seven samples were obtained from the core material opened and sampled under subdued red-light, with two further samples taken to account for

https://doi.org/10.5194/gchron-2023-27
Preprint. Discussion started: 9 January 2024

potential dose-rate inhomogeneity due to the complex stratigraphy. The material for equivalent dose (D_e) determination was subsequently treated with 10% HCl (no reaction) and 30% H_2O_2 (partly heavy reaction) to remove carbonates and organic matter, respectively. For the lowermost sample, only feldspar from the sand fraction (90-200 µm, CG) was extracted, whereas for the three top samples polymineral fine-grains (4-11 µm, FG) were used (based on grain-size distributions). For the remaining three samples, it was possible to extract both fractions.

Measurements were done on a Freiberg Instruments Lexsyg Research (Richter et al., 2013), equipped with a ET935QB photomultiplier (Hamamatsu Photonics) and using the combination of a Schott BG39 (3 mm) and a 414/46 BrightLine HC interference filter (3.5 mm) for detection. For all samples, a standard IRSL protocol was applied. For fine-grains, a post-IR (pIR) infrared stimulated luminescence (IRSL) protocol was additionally tested to potentially overcome the need for fading correction. The latter used a preheat at 250°C for 60 s, followed by IRSL stimulation at 50°C for 100 s (IR-50) and a subsequent second stimulation at 225°C for 100 s (pIR), whereas the latter step was omitted in the IRSL protocol. For fine-grains, the five replicate measurements are considered sufficient due to the excellent reproducibility, whereas for the sand fraction 20 replicate measurements were performed. Tests on quartz optically stimulated luminescence revealed no suitable signal, similar to reports on other directly bedrock derived samples (e.g., Preusser et al., 2006) and experience from the nearby Upper Rhine Graben (Preusser et al., 2016, 2021). For most samples, the average dose was calculated by the Central Age Model (CAM). In two cases, where the overdispersion exceeded 20%, the Minimum Age Model (MAN) was allied with a *sigma_b* value of 0.20 (Galbraith and Roberts, 2012). For IRSL and IR-50, a fading correction was undertaken using a g-value of 3.7±0.2 g per decade.

The concentration of dose-rate relevant elements was determined using a high-resolution gamma spectrometer, as outlined in Preusser et al. (2023). An alpha efficiency of 0.07±0.02 and an internal K-content of 12.5±1.0% (Huntley and Baril, 1997) were assumed. It has to be noted that the setting is particularly challenging with regard to dose rate determination. While average sediment moisture during burial time was estimated based on the water content measured directly after opening the cores in the laboratory, it has to be considered that a certain loess of water may have occurred during and after the coring operations. Furthermore, the deposits will have compacted after initial deposition due to the increase of load with time. Hence, the water used in the calculations are higher that the measured but still only represent an approximation. All age calculations were performed with the ADELEv2017 software (Degering and Degering, 2020). As the different sediment layers are partly quite thin, three-layer models were used for all samples, as implemented in ADELEv2017. Namely, for each layer an individual dose rate was calculated from which the effective dose rate acting on the sample area was determined. In addition, evidence for significant radioactive disequilibrium in the Uranium decay chain was observed for most of the samples. This is common in organic-rich deposits (e.g., Preusser and Degering, 2007; Preusser et al., 2023) and reflects the absorption of Uranium by humic substances from water (cf., Ivanovich and Harmon, 1992). This was accounted for in the dose rate calculations for each individual layer assuming a constant uptake of Uranium since the time of deposition. Both the

https://doi.org/10.5194/gchron-2023-27
Preprint. Discussion started: 9 January 2024

applied layer model and correction of radioactive disequilibrium represent only approximations to the real situation, as it is unfeasible to determine the detailed 3D geometry of the deposits, and the exact timing of Uranium uptake.

3.4 Local ^{10}Be production rate calibration and CRE dating of moraines

3.4.1 Fieldwork, sample preparation, and measurements

For establishing the BF production rate, we obtained rock samples (Table 2) from gneiss boulders on (i) the moraine that delimits the Feldsee Bog to the east, on (i) the ice-marginal moraine that has been partly buried by the bog's sediments, and on the (ii) moraine that dams up Lake Feldsee. We also sampled one boulder on the ice-marginal moraine at position FS-01 for CRE age calculations.

Table 2: Location of the sampled moraine boulders and their height, thickness of the rock samples, and topographic shielding at the sampling sites.

Sample	*xy* coordinates (WGS 1984 coordinate reference system)		Elevation (m a.s.l.)	Boulder height (m)	Sample thickness (cm)	Topographic shielding factor
	Latitude (° N)	Longitude (° E)				
FS-01a	47.872193	8.033919	1128	1.6	1.5	0.958616
FS-02a	47.872164	8.035611	1113	1.1	2.4	0.947912
FS-02b	47.871428	8.037746	1103	0.9	2.6	0.987496
FS-02c	47.869931	8.036674	1108	1.4	2.0	0.987583
FS-02d	47.870075	8.037022	1107	1.8	1.9	0.988521
FS-03a	47.869613	8.037770	1108	2.2	2.1	0.989194
FS-03b	47.869690	8.037641	1112	2.5	2.1	0.954505
FS-03c	47.869732	8.037687	1110	3.9	1.9	0.985596
FS-03d	47.871280	8.038474	1099	0.9	2.0	0.989967
FS-03e	47.870467	8.038263	1106	2.0	2.4	0.960224
FS-03f	47.870475	8.038298	1106	2.2	2.8	0.985626

As the study of Tomkins et al. (2021) demonstrated that landform stability mainly influences the scatter in age distributions from moraines (and thus in ^{10}Be concentrations), only well-embedded boulders were selected to avoid underestimated ^{10}Be concentrations due to boulder rotating as well as post-depositional and post-stabilisation exhumation. Previous sampling

https://doi.org/10.5194/gchron-2023-27
Preprint. Discussion started: 9 January 2024

guidelines suggested that flat-topped boulders should be selected for CRE dating of moraines (e.g., Ivy-Ochs and Kober, 2008). However, none of the moraine boulders in the study area was flat-topped, thus a total of 11 rock samples (Table 2) was obtained with an angle grinder, a chisel, and a hammer from dipping surfaces with a constant angle. Masarik and Wieler (2003) argued that the cosmic ray flux on non-flat rock surfaces is lower than on flat rock surfaces, since the number of scattered neutrons is larger in non-flat rock surfaces. Due to these potential edge effects, rock surfaces near boulder edges were avoided during fieldwork. As scaling of the ^{10}Be production rate to sampling sites required coordinates of the sampling sites, *xy*-coordinates of the boulders were recorded with a global navigation satellite system (Leica CS20 controller and Leica Viba GS14 antenna). Obtaining pairs of azimuth and elevation angles of the horizon around the sampling sites for topographic shielding factor calculations was not possible at all sampling sites due to dense forest cover. Therefore, the ArcGIS toolbox of Li (2018) was chosen for shielding factor calculations. Following the guidelines of Hofmann (2022), the high-resolution DEM of the study site (LGL, 2015) was resampled to a *xy*-resolution of 30 m. The mass and thickness of each rock fragment in the samples was determined to compute the mass-weighted average of the sample's thickness. See the supplement for a detailed sample documentation.

Quartz separation and ^{10}Be extraction from purified quartz was accomplished in the laboratory facilities of the University of Freiburg (Germany) and the Laboratoire National des Nucléides Cosmogéniques (LN_2C) in Aix-en-Provence (France) according to the protocol described in Hofmann et al. (2023). After crushing, and wet sieving (target grain size: 0.25 – 1 mm), the samples were passed through a magnetic separator (S.G. Frantz Co.). The samples were then treated with mixtures of 37% HCl and 35% H_2SiF_6 to further isolate quartz and remove feldspars. Because the samples still contained feldspar after this treatment, the samples were subsequently etched with diluted 5.5% HF, dried, spiked with magnetite powder (325 mesh), and passed through a magnetic separator. Meteoric ^{10}Be was removed with 48% HF in three steps, with 10% of the quartz dissolved in each step. A dose of about 150 mg of a ^{9}Be carrier solution (3025±9 µg ^{9}Be g^{-1}) was added to each sample before total dissolution with 48% HF. Chromatography with anionic and cationic exchange resins (DOWEX 1X8 and 50WX8), as well as precipitation stages were then performed to further separate and purify beryllium. To thermally decompose the final $Be(OH)_2$ precipitate to BeO, the samples were subsequently heated to 700 °C. The samples were finally mixed with Nb and pressed into copper cathodes for AMS measurements.

The ^{10}Be concentrations in the samples were deduced from AMS measurements at ASTER (Accélérateur pour les Sciences de la Terre, Environnement, Risques; Arnold et al., 2013), the French AMS national facility, at CEREGE (Centre Européen de Recherche et d'Enseignement des Geosciences de l'Environnement) in Aix-en-Provence (France). The measured ^{10}Be/^{9}Be ratios were normalised with respect to the in-house standard STD-11 using an assigned ^{10}Be/^{9}Be ratio of (1.191±0.013) × 10^{-11} (Braucher et al., 2015) and the Be half-life of (1.387±0.012) × 10^{6} years (Chmeleff et al., 2010; Korschinek et al., 2010). For the calculation of the ^{10}Be/^{9}Be ratio uncertainties, (i) the measurement uncertainty (counting statistics), (ii) the uncertainty of average standard measures, and (iii) the systematic error of ASTER (0.5%; Arnold et al., 2010) were taken

https://doi.org/10.5194/gchron-2023-27
Preprint. Discussion started: 9 January 2024

into account. The ^{10}Be concentrations in the samples were corrected for the ^{10}Be concentration in a batch-specific chemical blank.

3.4.2 Production rate calibration

The calibration of the ^{10}Be BF production rate followed the workflow of Martin et al. (2017, their Fig. 3). Following equation 4 in Martin et al. (2017), the ^{10}Be concentration in each sample was first corrected for the sample thickness and for topographic shielding to compute a theoretical ^{10}Be concentration in a sample with null thickness. The ^{10}Be concentrations were then scaled to the mean latitude, longitude, and elevation representative for all sampled boulders. Following the guidelines of Ross (2003), the ^{10}Be concentrations were subsequently evaluated with the criterion of Peirce, and a weighted ^{10}Be concentration was computed after the exclusion of outliers. The mean squared weighted deviation (MSWD) for the ^{10}Be concentrations turned out to be higher than one. As recommended by Martin et al. (2017), the standard error of the weighted mean ^{10}Be concentration was multiplied with $\sqrt{MSWD}$ to obtain the uncertainty of the average ^{10}Be concentration.

The local ^{10}Be production rates for the study site were calculated with the aid of CREp, available at https://crep.otelo.univ-lorraine.fr (last access: 6 November 2023). For calibration, the modelled basal age of the lake sediments above the moraine at ice-marginal position FS-02 was converted into ka before 2010 CE. The local ^{10}Be production rates were computed for all scaling schemes and geomagnetic databases available in CREp. Following the approach in a previous calibration study (Fenton et al., 2011) and several other calibration studies (e.g., Stroeven et al., 2015), a "baseline" production rate was first calculated, i.e., a production rate that accounts for the snow cover, vegetation cover, soil cover, and postdepositional weathering bias at the study site. As many geomorphologists prefer to work with version 3 of the online exposure age calculator, formerly known as the CRONUS-Earth online exposure age calculator (available at http://hess.ess.washington.edu/math/v3/v3_cal_in.html, last access: 8 November 2023), the "baseline" production rate was also determined with this calculator. See the supplement for the input-sheet.

Fenton et al. (2011) argued that snow cover and post-depositional weathering of sampling surfaces probably affected their local ^{10}Be production rates at two rock avalanches in Norway, and proposed postdepositional-weathering- and snow-cover-corrected local production rates. The sampling sites in the southern Black Forest are situated in a heavily forested and sheltered area. A few centimetre-thick organic soil, mosses, and shrubs, most notably blueberry bushes (*Vaccinium myrtillus)* covered the sampled boulders. As soil cover on boulders leads to enhanced chemical weathering rates (cf., Ahnert, 2009), the boulders probably underwent significant postdepositional weathering. In addition, snow cover during winter has probably slowed down the accumulation of ^{10}Be in quartz in the sampled boulders. During field surveys in 2022 CE, we observed a substantial snow cover in winter on the boulders, being up to a few decimetres thick.

https://doi.org/10.5194/gchron-2023-27
Preprint. Discussion started: 9 January 2024

Therefore, proposing a postdepositional-weathering- and snow-cover-corrected local ^{10}Be production rate was deemed mandatory. Reuther (2007) inferred a postdepositional weathering rate (0.24 cm ka^{-1}) for a similar setting in the Bavarian Forest (recalculated from Reuther, 2007 with the CREp program and the parameters listed above), based on ^{10}Be concentration in samples from protruding quartz veins with striae on glacially polished bedrock. As we deemed this postdepositional weathering rate internally robust and representative for the study site, it was selected for the calibration of the weathering-corrected production rate. According to data from the weather station of the DWD in the municipality of Schluchsee (at 990 m a.s.l.), situated about 10 km to the SE of the study area, seasonal cover lasted for four months in the 1961-1990 CE period (average snow depth: 0.3 m; DWD, 2023). Assuming similar conditions during the whole duration of exposure, a snow density of 0.3 g cm^{-3}, an attenuation length for fast neutrons in snow of 109 g cm^{-2} (Zweck et al., 2013), the commonly used equation 3.76 in Gosse and Phillips (2001) yielded a snow shielding factor of ~0.974. This factor was incorporated this factor during production rate calibrations.

Modelling has revealed up to a 7% reduction in the intensity in cosmic ray flux in old-growth temperate forests (Plug et al., 2007). As the sampled moraine boulders were situated in forested areas, a vegetation-corrected production rate was calculated. According to palynological data from several bogs and fens in the Black Forest, the timberline rose to an elevation of ≥1100 m a.s.l. during the last interstadial of the Late Pleistocene (Fig. 5a, Lang, 2006), commonly referred to as Allerød interstadial (13.9 – 12.8 ka; Heiri et al., 2014). During this period, open pine-birch forests probably covered the study site (Fig. 5b). The presence of *Pinus* in the pollen record, however, does not necessarily indicate that the study site was forested. As discussed by Andrieu et al. (1997), *Pinus* generally tends to be overrepresented in pollen records due to high pollen production and winds easily transport the pollen over long distances. Unfortunately, Lang (2005) did not observe *Pinus* or *Betula* macro-remains that would have more convincingly supported the idea of open pine-birch forests. Lang (2006) suggested that the timberline shifted back to about 750 m a.s.l. during the subsequent cold phase (Fig. 5a), often referred to as Younger Dryas stadial (12.8 – 11.7 ka; Heiri et al., 2014). However, with regard to the Northern Alps where the timberline lowered by about 200 m during this cold phase (cf., Stojakowits et al., 2014), the reconstructed shift of the timberline in the Black Forest (c. 350 m) appears quite strong. It is therefore possible that the study site remained a sparsely forested area (Stojakowits, P., pers. comm., 25 October 2023). Since we could not conclusively clarify the Lateglacial vegetation history of the study site, we assumed for the vegetation correction that forests covered the study area throughout the duration of exposure. We are, however, aware that this correction might overestimate the impact of the vegetation on the cosmic ray flux at the sampling sites. For the vegetation correction, we assumed a shielding factor of 0.98 for boreal forests (Plug et al., 2007), the probably best analogues for the forests at the study site.

https://doi.org/10.5194/gchron-2023-27
Preprint. Discussion started: 9 January 2024

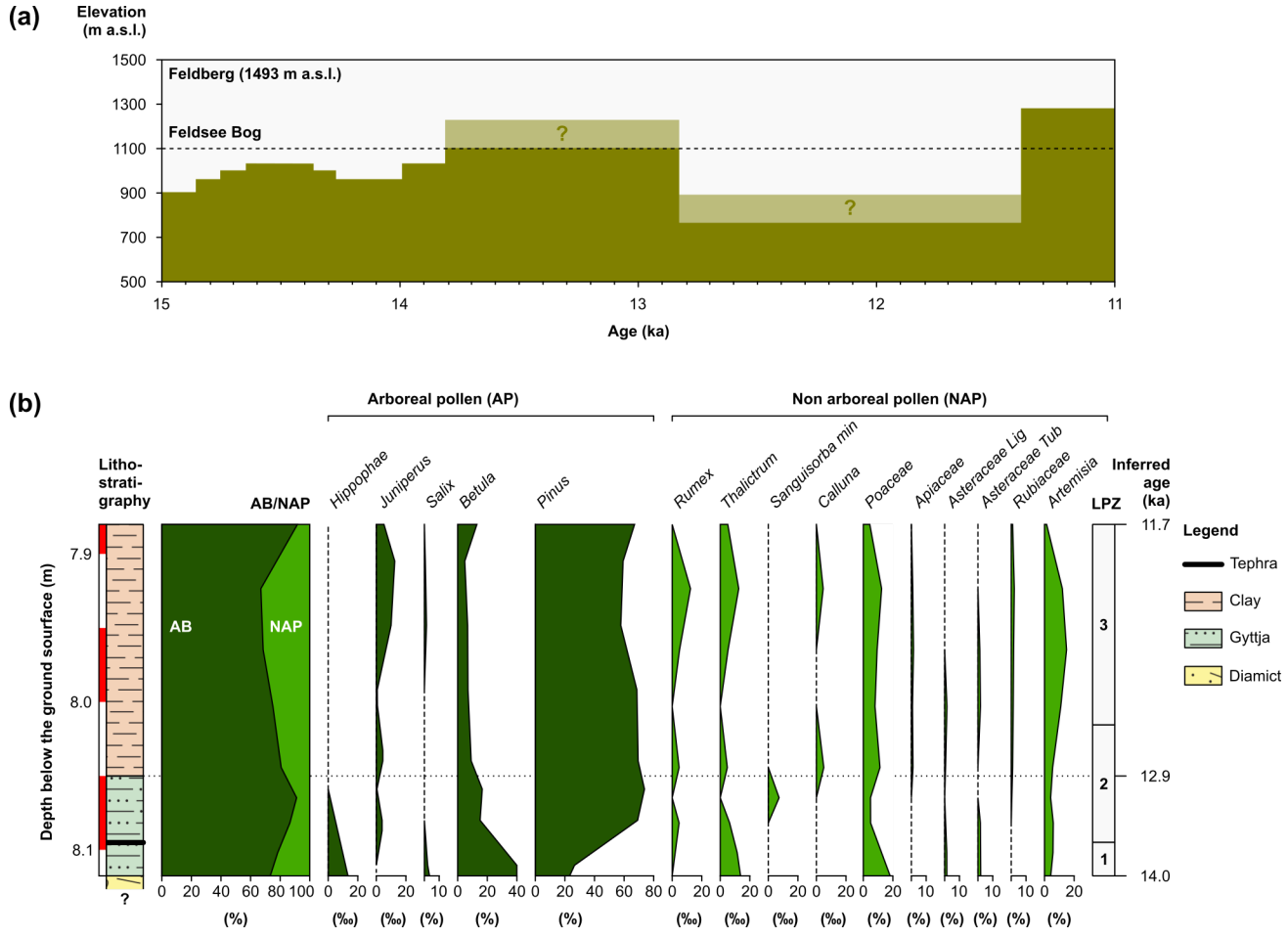

Figure 5: (a) Evolution of the timberline in the Black Forest between 15 ka and 11 ka (redrawn from Lang, 2006). (b) Succession of sediment in the sediment core 5 from the Feldsee Bog (Fig. 4), inferred ages of the sediments, and vegetation dynamics, as documented in the pollen record. LPZ: local pollen zones. Redrawn from Lang (2005).

3.4.3 CRE age calculations and statistical assessment

Hofmann et al. (2022) recently recalculated all CRE ages for the mid-elevation mountain ranges of Central Europe with the Chironico landslide spallogenic production rate [4.10±0.10 atoms ^{10}Be g^{-1} quartz a^{-1} at sea-level and high latitudes (SLHL); Claude et al., 2014]. To assess the effect of the choice of the production rate, CRE ages, internal (analytical) uncertainties, and external uncertainties (i.e., analytical uncertainties plus the error of the ^{10}Be production rate added in quadrature) were calculated in CREp with both the Chironico production rate and the BF production rate. See Table S20 for the input-table. The following parameters were chosen to scale the SLHL production rates to the sampling sites: time-dependent 'Lm' scaling (Nishiizumi et al., 1989; Lal, 1991; Stone, 2000; Balco et al., 2008) and the ERA atmosphere model (Uppala et al., 2005), as recommended by Martin et al. (2017). In CREp, the ages were corrected for changes in the Earth's magnetic field with data from the atmospheric ^{10}Be-based geomagnetic database (Muscheler et al., 2005). Since the sampled moraine

https://doi.org/10.5194/gchron-2023-27
Preprint. Discussion started: 9 January 2024

boulders were derived from quartz-rich lithologies, the density of quartz (2.65 g cm^{-3}) was assumed for the thickness correction.

Multiple ages were available for most of the moraines. The assessment of the ages followed the guidelines of Balco (2023). If three or more ages were available from the same landform, reduced chi-squared ($\chi^2{}_R$) was computed. $X_R{}^2$ was then compared with a critical value from a standard χ^2-table (degree of freedom: $n - 1$). The confidence interval was set to 95%. If $\chi^2{}_R$ turned out to be lower than the critical value, the hypothesis that the data formed a single population was at 95% confidence (cf., Balco, 2011). In this case, the landform age was determined by computing the error-weighted mean. If $\chi^2{}_R$ turned out to be higher than the critical value, implying that measurement uncertainties did not fully account for scatter in ages from the same landform (cf., Balco, 2011), the age that was furthest from the average age in relation to its measurement uncertainty was considered an outlier and removed from the dataset. This procedure was repeated until the pruned dataset yielded an acceptable $\chi^2{}_R$ value. Not more than half of the ages from the same landform were excluded. The procedure was also stopped if three ages were remaining. If the original or pruned datasets yielded a p-value > 0.05, the internal landform uncertainty was determined by calculating the standard error. If the original or pruned datasets gave a p-value < 0.05, the standard deviation of the ages was selected as internal landform age uncertainty. The external landform age uncertainties were calculated by adding the internal landform age uncertainties and the error of the selected production rate in quadrature.

5. Results

5.1 Lithostratigraphy of the sediment sequence

The percentage of sediment recovery increased from 67% between a depth of 4 and 5 m to 81% between a depth of 5 and 6 m. Borehole FSM recovered the sedimentary succession of the Feldsee Bog and the uppermost 0.32 m of the partly buried moraine at position FS-02 (Fig. 6).

In the lowermost 0.32 m, this succession consisted of greenish grey, medium-densely packed silty diamicts that were mostly clast-supported and occurred in a fining-upwards package. Individual clasts were angular to subangular, and of diverse crystalline lithologies of local origin (gneiss, migmatite and granite porphyry). With 1.2% to 1.9%, LOI values in samples from the sandy diamicts at a depth of 5.80–5.68 m were very low. At a depth of 5.68 m, the diamicts transitioned into crudely laminated light grey to olive grey fines, silt, and clay, that contained dispersed coarse sand to fine gravel clasts at their base. LOI values varied between 1.7% and 10.5 %. Dark brown to grey fines, silt, and clay overlay these deposits. LOI values ranged from 12.3% to 35.7%. Macroscopic plant fragments as well as a distinct 2-3 mm-thick light-grey lamina at a decompacted depth of 4.91 m occurred in this unit. Light beige grey fines (sand, silt, and clay) with low LOI

https://doi.org/10.5194/gchron-2023-27
Preprint. Discussion started: 9 January 2024

values (4.9–5.6 %) overlay the dark brown to grey fines. The basal contact of this unit was sharp. Starting at a depth of 4.75 m, organic-rich (LOI: 30.5–54.8%) gyttja-type deposits occurred that were crudely bedded on a cm-scale (Fig. 6).

The succession of FSM (Fig. 6) reflects the glacial-postglacial transition of the study area. The borehole was situated in elongation of a geomorphologically distinct ice-marginal moraine (Fig. 3) and recovered its continuation into the Feldsee Bog. The corresponding diamicts (6.00-5.68 m) were medium-densely packed and contained washed-out sections with decreased fines content. This indicates an origin from melt-out and subaqueous mass movements (e.g., Schlüchter, 1997).

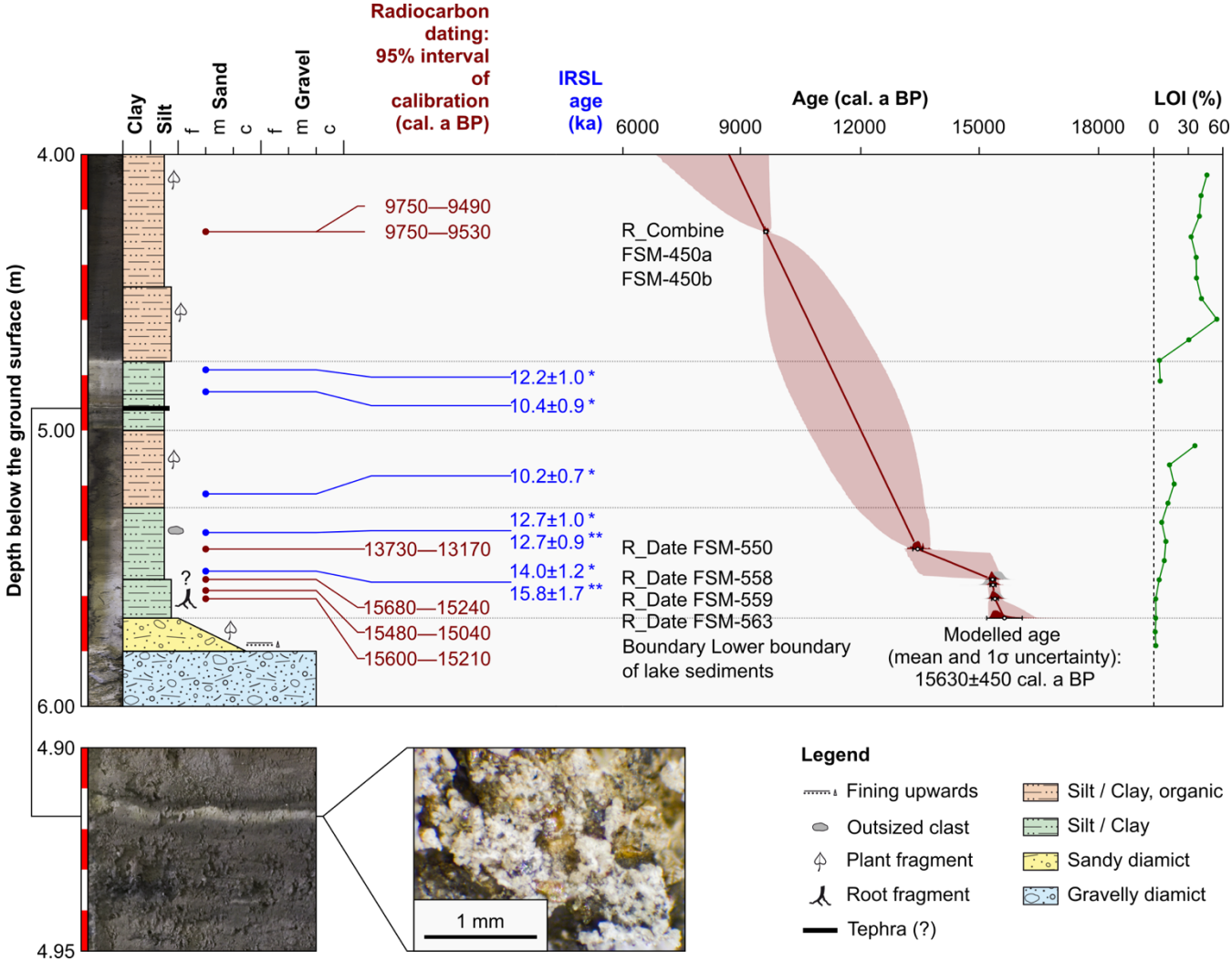

Figure 6: Photos of the sediment cores from the Feldsee Bog acquired with the methodology of Gegg and Gegg (2023), sediment succession, radiocarbon and luminescence ages, and the age-depth model. The probability density for each calibrated age is shown with light grey filled curves and the modelled posterior probability functions are shown with darkred filled curves. The age-depth model in light blue is plotted at a 95.4% confidence level. *fine-grains. **coarse-grains.

https://doi.org/10.5194/gchron-2023-27
Preprint. Discussion started: 9 January 2024

The decreasing gravel content in this cycle further suggests a progressive shift from an immediately ice-proximal to a slightly more distal position due to glacier retreat. Well-sorted basin fines abruptly overlay the basal diamicts, reflecting a cessation of direct glacial input, although dispersed outsized clasts near the bottom have likely been deposited as ice-rafted debris. Frequently occurring plant fragments and fibres, and higher LOI values indicate that a milder climate prevailed during the emplacement of the sediments. Just like Lang (2005), we observed a light-grey lamina in the same stratigraphical position. Although the stratigraphical position clearly speaks for the Laacher See Tephra interpretation, there is a need for further mineralogical investigations to confirm this working hypothesis. A mostly inorganic package at 5.00-4.75 m followed the first organic-rich package from 5.28 m to 5.00 m, possibly due to cooler climatic conditions. The emplacement of the gyttja-type sediments above 4.75 m depth occurred during persistently temperate conditions.

5.2 Radiocarbon ages and age-depth model

Table 3 summarises conventional ^{14}C ages and calibrated radiocarbon ages. See also Fig. 6. Following the recommendation of Millard (2014), 95% ranges of calibration are given.

Table 3: Results of radiocarbon dating of macrofossils in sediment cores from the Feldsee Bog.

Sample	Decompacted depth (m)	Conventional age (^{14}C a BP)	Calibrated age range (cal. a BP)
FSM-450a	4.28	8620 ± 60	9750—9490
FSM-450b	4.28	8650 ± 50	9750—9530
FSM-536	5.24	720 ± 30	-
FSM-538	5.26	Modern	-
FSM-550	5.43	11540 ± 120	13730—13170
FSM-553	5.47	Modern	-
FSM-558	5.54	12930 ± 70	15680—15240
FSM-560	5.56	12770 ± 60	15480—15040
FSM-563	5.61	12880 ± 60	15600—15210

Calibrating ^{14}C ages of unidentified plant fragments sampled at decompacted depths of 5.61 m, 5.56 m, and 5.54 m resulted in overlapping ages of 15600—15210 cal. a BP, 15480—15040 cal. a BP, 15680—15240 cal. a BP, respectively. Sphagnum moss at a decompacted depth of 5.53 m yielded a modern ^{14}C age. Leaf fragments at a depth of 5.43 gave an age of 13730—13170 cal. a BP. Sphagnum moss at a decompacted depth of 5.26 m yielded a ^{14}C age of 720±30 a BP, whereas unidentified plant fibre at a decompacted depth of 5.24 m gave a modern ^{14}C age. In contrast to the FSM-563, FSM-560, and FSM-558

https://doi.org/10.5194/gchron-2023-27
Preprint. Discussion started: 9 January 2024

samples, the appearance of sphagnum moss (FSM-553 and FSM-538 samples) and the plant fibre (FSM-536) was comparably fresh and thus the macrofossils are probably modern samples that were squeezed into older sediments during vibracoring. As these macrofossils apparently were modern samples, their ^{14}C ages were not included in the age-depth model. Macrofossils sampled at a depth of 4.28 m gave almost identical ages of 9750—9530 cal. a BP and 9750—9490 cal. a BP, respectively.

Figure 6 shows the age-depth model for the depth between 5.68 m and 4.00 m. The agreement index of the model turned out to be 70%, exceeding the critical threshold of 60% advocated by Bronk Ramsey (2008). According to this model, the deposition of lake sediments commenced at 16460—15220 cal. a BP (mean age and 1σ uncertainty: 15630±450 cal. a BP), thus providing the minimum age of ice-free conditions which will just post-date the glacier recession from positions FS-02 and FS-03. Including the age of the supposed Laacher See Tephra (13006±9 cal. a BP; Reinig et al., 2021) in the age model would have led to an almost identical deglaciation age (15640±490 cal. a BP).

5.3 Luminescence ages

Table 4 summarises the luminescence data. Whereas in the lower part of the sequence (samples FSM-3 to FSM-5), the pIR ages are some 25% higher than the fading corrected IRSL and IR-50 ages, there is a good agreement between the different approaches for the two samples taken just above the apparent Laacher See Tephra (samples FSM-1 and FSM-2). The mean age for these latter samples is 11.4±0.4 ka, which is some 10-15 % lower than expected for sediment above the tephra (~13 ka). FSM-3 is also slightly to moderately underestimating the tephra age with estimates of 10.2±0.7 ka (IRSL) and 11.7±1.0 ka (IR-50). The ages for sample FSM-4 (FG: IRSL =12.7±1.0 ka, IR-50 = 13.2±1.0; CG: 12.7±0.9 ka) overlap with the radiocarbon age of ca. 13.4 ka. The same applies to the basal sample FSM-5, with ages of 14.0±1.2 ka (FG: IRSL), 14.2±1.2 ka (FG: IR-50), and 15.8±1.7 (CG: IRSL). Overall, there is a tendency of slightly lower IRSL/IR-50 ages compared to independent age control through radiocarbon dating. This is possibly explained by a slightly too low assumed sediment moisture due to compaction of the deposits with time, uncertainties related to the applied layer model, and/or correction of radioactive disequilibrium (timing of Uranium uptake). On the other hand, some the pIR ages appear slightly overestimated with might be related to small residual signal levels at the time of deposition. However, the consistent results determined for sample FSM 4 indicate that fading correction is appropriate. Figure 6 only displays the IRSL ages for simplification.

https://doi.org/10.5194/gchron-2023-27
Preprint. Discussion started: 9 January 2024

Table 4: Results of luminescence dating of samples from the sediment cores from the Feldsee Bog. Depth refers to the depth below surface after decompaction. Stim.: stimulation used for Equivalent Dose (D_e) determination. Given are the measured water content (W) and the sediment moisture (Mois.) used for dose rate calculations. The activity of different isotopes (K, Th, U-238, Ra-226) is given, revealing disequilibrium in the Uranium decay chain. *n*: number of replicate D_e measurements, Model: applied approach to extract mean De (CAM: Central Age Model; MAM: Minimum Age Model).

Lab code	Depth (m)	Stim.	W (%)	Mois. (%)	K (Bq kg^{-1})	Th (Bq kg^{-1})	U-238 (Bq kg^{-1})	Ra-226 (Bq kg^{-1})	Dose rate (Gy ka^{-1})	*n*	OD (%)	Model	D_e (Gy)	Age (ka)
FSM-D1	473-478	-	80	100±10	230±40	51±5	490±40	59±5	-	-	-	-	-	-
FSM1-FG	483-488	IRSL	42	60±5	880±100	81±6	174±19	92±7	4.55±0.37	5	1	CAM	36.67±0.55	12.2±1.0
		IR-50								4	0	CAM	37.17±0.49	11.5±1.0
		pIR							4.61±0.38	4	0	CAM	55.19±0.75	11.9±1.0
FSM2-FG	488-493	IRSL	46	60±5	640±80	85±7	201±22	100±5	4.77±0.40	5	2	CAM	35.33±0.59	10.4±0.9
		IR-50								5	2	CAM	36.42±0.54	10.7±0.9
		pIR								5	0	CAM	56.77±0.69	11.8±1.0
FSM-D2	523-528	-	76	100±10	310±50	57±5	260±30	73±7	-	-	-	-	-	-
FSM3-FG	533-538	IRSL	64	80±5	490±60	66±5	282±26	98±7	3.74±0.34	5	8	CAM	27.33±1.04	10.2±0.7
		IR-50								5	0	CAM	31.48±0.58	11.7±1.0
		pIR								5	2	CAM	55.38±0.89	14.1±1.2
FSM4-FG	543-548	IRSL	51	70±5	640±70	67±5	215±20	84±6	4.02±0.32	5	3	CAM	36.49±0.75	12.7±1.0
		IR-50								5	0	CAM	38.42±0.76	13.2±1.0
		pIR								5	2	CAM	61.17±1.28	15.3±1.2
FSM4-CG		IRSL							3.45±0.22	20	32	MAM	30.99±1.57	12.7±0.9
FSM5-FG	553-558	IRSL	46	55±5	680±70	67±5	233±20	80±5	5.65±0.46	5	0	CAM	45.33±0.60	14.0±1.2
		IR-50								4	2	CAM	46.41±0.76	14.2±1.2
		pIR								4	0	CAM	78.12±1.08	17.6±1.3
FSM5-CG		IRSL							3.96±0.41	20	24	MAM	44.28±4.28	15.8±1.7

5.4 Beryllium-10 concentrations in rock samples from moraine boulders

Table 5 summarises the results of AMS measurements and ^{10}Be concentrations in rock samples from moraine boulders. During AMS measurements on the FS-03b sample, ^{9}Be currents were very low, decreasing from 0.1 to 1 µA during AMS measurements. Hence, the ^{10}Be concentration in the sample from the boulder should be considered with greatest caution.

https://doi.org/10.5194/gchron-2023-27
Preprint. Discussion started: 9 January 2024

Table 5: Characteristics of the samples, ^{9}Be added, and the results of AMS measurements. ^{10}Be concentrations in the samples were corrected with the ^{10}Be concentration in a batch-specific blank. *Analytical blank. **Due to low ^{9}Be currents during AMS measurements, the reported ^{10}Be concentration should not be regarded as reliable.

Sample	Mass of dissolved quartz (g)	Beryllium-9 added ($\times 10^{19}$ atoms)	Beryllium-10/ Beryllium-9 ratio ($\times 10^{-14}$)	Beryllium-10 concentration (atoms g^{-1} quartz)
BK-FS-SH-WH-WK*	-	3.03	0.139 ± 0.032	-
FS-01a	12.0489	3.00	5.54 ± 0.18	134500 ± 4700
FS-02a	9.9458	3.03	4.60 ± 0.17	135800 ± 5300
FS-02b	26.1755	3.05	12.21 ± 0.45	140600 ± 5300
FS-02c	21.7892	3.03	10.37 ± 0.32	142100 ± 4600
FS-02d	16.0494	3.02	5.05 ± 0.22	92300 ± 4200
FS-03a	2.0943	3.03	1.25 ± 0.08	161000 ± 13000
FS-03b	13.1496	3.03	5.26 ± 0.70	118000 ± 16000 **
FS-03c	21.2975	3.03	10.10 ± 0.31	141500 ± 4600
FS-03d	16.2466	3.02	7.32 ± 0.24	133300 ± 4700
FS-03e	10.2760	3.02	5.05 ± 0.18	144100 ± 5400
FS-03f	9.1148	3.01	4.60 ± 0.19	147400 ± 6400

5.5 Local ^{10}Be production rate

For the reason outlined in the previous section, the ^{10}Be concentration in the FS-03b sample was not used for determining the BF production rate. Correcting the ^{10}Be concentrations for topographic shielding and the sample thickness led, in most cases, to minor shifts in the ^{10}Be concentrations in samples. Table 6 exemplifies the normalisation procedure for time-dependent Lal/Stone scaling and the geomagnetic database of Muscheler et al. (2005). During the evaluation of the set of ^{10}Be concentrations with the criterion of Peirce, the ^{10}Be concentration in the sample from the FS-02d moraine boulder turned out to be an outlier. Hence, weighted mean concentrations were computed with the ^{10}Be concentrations in the remaining samples. In all cases, MSWD exceeded the critical value of one (see Martin et al., 2017 for further discussion), and, therefore, the standard error of the weighted mean and $\sqrt{MSWD}$ were added in quadrature to obtain the uncertainties of the weighted mean ^{10}Be concentrations.

https://doi.org/10.5194/gchron-2023-27
Preprint. Discussion started: 9 January 2024

Table 6: ^{10}Be concentrations in sampled moraine boulders, normalised ^{10}Be concentrations (null sample thickness, no shielding) and scaling factors. *The ^{10}Be concentration was classified as an outlier with the criterion of Peirce.

Sample	Beryllium-10 concentration (atoms g^{-1} quartz)	Normalised ^{10}Be concentration (atoms g^{-1} quartz)	Scaling factor (time-dependent Lal/Stone scaling)
FS-02a	135800 ± 5300	146100 ± 5300	2.58
FS-02b	140600 ± 5300	151600 ± 5300	2.56
FS-02c	142100 ± 4600	146300 ± 4600	2.57
FS-02d	92300 ± 4200 *	94900 ± 4200 *	2.58
FS-03a	161000 ± 13000	165000 ± 13000	2.58
FS-03c	141500 ± 4600	145400 ± 4600	2.59
FS-03d	133300 ± 4700	136900 ± 4700	2.56
FS-03e	144100 ± 5400	153100 ± 5400	2.58
FS-03f	147400 ± 6400	146100 ± 6400	2.58

Table 7 reports the BF production rate for the different scaling schemes and geomagnetic databases in CREp. We obtained a "baseline" BF ^{10}Be production rate between 3.62±0.12 and 3.67±0.12 atoms ^{10}Be g^{-1} quartz a^{-1} at SLHL for the different scaling schemes and geomagnetic databases in CREp. These production rate resembled the production rate for 'Lm' scaling, calculated with version 3 of the online exposure age calculator, formerly known as the CRONUS-Earth online exposure age calculator (3.65±0.20 atoms ^{10}Be g^{-1} quartz a^{-1} at SLHL). Removing the snow cover bias at the study site led to a 2.7% higher production rate between 3.72±0.12 and 3.77±0.12 atoms ^{10}Be g^{-1} quartz a^{-1} at SLHL. The snow-shielding- and postdepositional-weathering-corrected production rate ranged from 3.84±0.13 to 3.89±0.13 atoms ^{10}Be g^{-1} quartz a^{-1} at SLHL and was thus 6% higher than the "baseline" production rate. With 3.92±0.13 to 3.97±0.13 atoms ^{10}Be g^{-1} quartz a^{-1} at SLHL, the postdepositional-weathering-, snow-cover-, and forest-cover-corrected production rate was 8% higher than the "baseline" production rate (Table 7).

5.6 Beryllium-10 CRE ages

See Table 8 and Fig. 7 for CRE ages of moraine boulders, landform ages, and reduced χ^2 values. Table 8 reveals that the ages calculated with the BF production rate turned out to be, on average, 11.0% higher than those computed with the Chironico landslide production rate. We hereinafter only comment on the ages derived with the BF production rate and refer to external uncertainties.

The FS-03a, FS-03c, FS-03d, FS-03e, and FS-03f boulders on the ice-marginal moraine at position FS-03 yielded ages of 17.4±1.5 ka, 15.4±0.7 ka, 14.6±0.7 ka, 16.2±0.8 ka, and 16.2±0.9 ka, respectively. As mentioned above, the ^{10}Be

https://doi.org/10.5194/gchron-2023-27
Preprint. Discussion started: 9 January 2024

concentration in the sample from the FS-03b boulder should not be regarded reliable due to low ^{9}Be currents during Be AMS measurements and, thus, no age was calculated. The age of the FS-03d boulder (14.6±0.7 ka) was classified as an outlier. The remaining ages gave a landform age of 15.9±0.4 ka.

Table 7: The BF ^{10}Be production rate (atoms ^{10}Be g^{-1} quartz a^{-1} at SLHL) for different scaling schemes and geomagnetic databases available in CREp. For the references of the geomagnetic databases and scaling schemes in CREp, see Martin et al., 2017.

Scaling scheme	Time-dependent Lal/Stone			LSD		
Geomagnetic database	Atmospheric ^{10}Be-based virtual dipole moment (VDP)	LSD (Lifton-Sato-Dunai) framework	Lifton VDM 2016	Atmospheric ^{10}Be-based VDP	LSD framework	Lifton VDM 2016
"Baseline" production rate	3.66±0.12	3.62±0.12	3.64±0.12	3.67±0.12	3.65±0.12	3.64±0.12
Production rate (snow shielding bias removed)	3.76±0.12	3.72±0.12	3.74±0.12	3.77±0.12	3.75±0.12	3.74±0.12
Production rate (snow shielding and postdepositional weathering bias removed)	3.88±0.13	3.84±0.13	3.86±0.13	3.89±0.13	3.87±0.13	3.86±0.13
Production rate (snow shielding, postdepositional weathering, and forest cover bias removed)	3.96±0.13	3.92±0.13	3.93±0.13	3.97±0.13	3.94±0.13	3.94±0.13

https://doi.org/10.5194/gchron-2023-27
Preprint. Discussion started: 9 January 2024

Table 8: CRE ages of sampling surfaces on moraine boulders computed with the BF ^{10}Be production rate and Chironico landslide production rate (Claude et al., 2014). *Classified as an outlier. **Due to low ^{9}Be counts during AMS measurements, the ^{10}Be concentration in the sample is not reliable and, therefore, no CRE age was computed.

Ice-marginal position	Boulder	Beryllium-10 CRE age (ka before 2010) and internal uncertainty in ka [external uncertainty (ka) in parentheses]		Age difference (%)	Landform age (ka before 2010) and internal uncertainty in ka [external uncertainty (ka) in parentheses]		Reduced χ^2			
		BF production rate	Chironico landslide production rate		BF production rate	Chironico landslide production rate	Before the exclusion of outliers		After the exclusion of outliers	
							BF production rate	Chironico landslide production rate	BF production rate	Chironico landslide production rate
FS-01	FS-01a	14.77±0.51 (0.69)	13.30±0.46 (0.56)	11.1	14.93±0.50 (0.71)	13.30±0.46 (0.56)	-	-	-	-
FS-02	FS-02a	15.35±0.59 (0.77)	13.84±0.53 (0.62)	10.9	15.41±0.03 (0.51)	13.88±0.03 (0.50)	32.0	32.5	0.0	0.0
	FS-02b	15.42±0.57 (0.75)	13.88±0.51 (0.60)	11.1						
	FS-02c	15.44±0.49 (0.69)	13.91±0.44 (0.54)	11.0						
	FS-02d	10.10±0.45 * (0.55)	9.12±0.40 * (0.46)	10.7						
FS-03	FS-03a	17.43±1.39 (1.50)	15.65±1.23 (1.29)	11.4	15.89±0.43 (0.67)	14.32±0.64 (0.72)	2.6	2.5	1.4	1.3
	FS-03b	- **	- **	-						
	FS-03c	15.37±0.49 (0.69)	13.86±0.44 (0.54)	10.9						
	FS-03d	14.58±0.49 (0.68)	13.13±0.45 (0.55)	11.0						
	FS-03e	16.17±0.60 (0.79)	14.56±0.53 (0.63)	11.1						
	FS-03f	16.17±0.68 (0.86)	14.55±0.60 (0.69)	11.1						

https://doi.org/10.5194/gchron-2023-27
Preprint. Discussion started: 9 January 2024

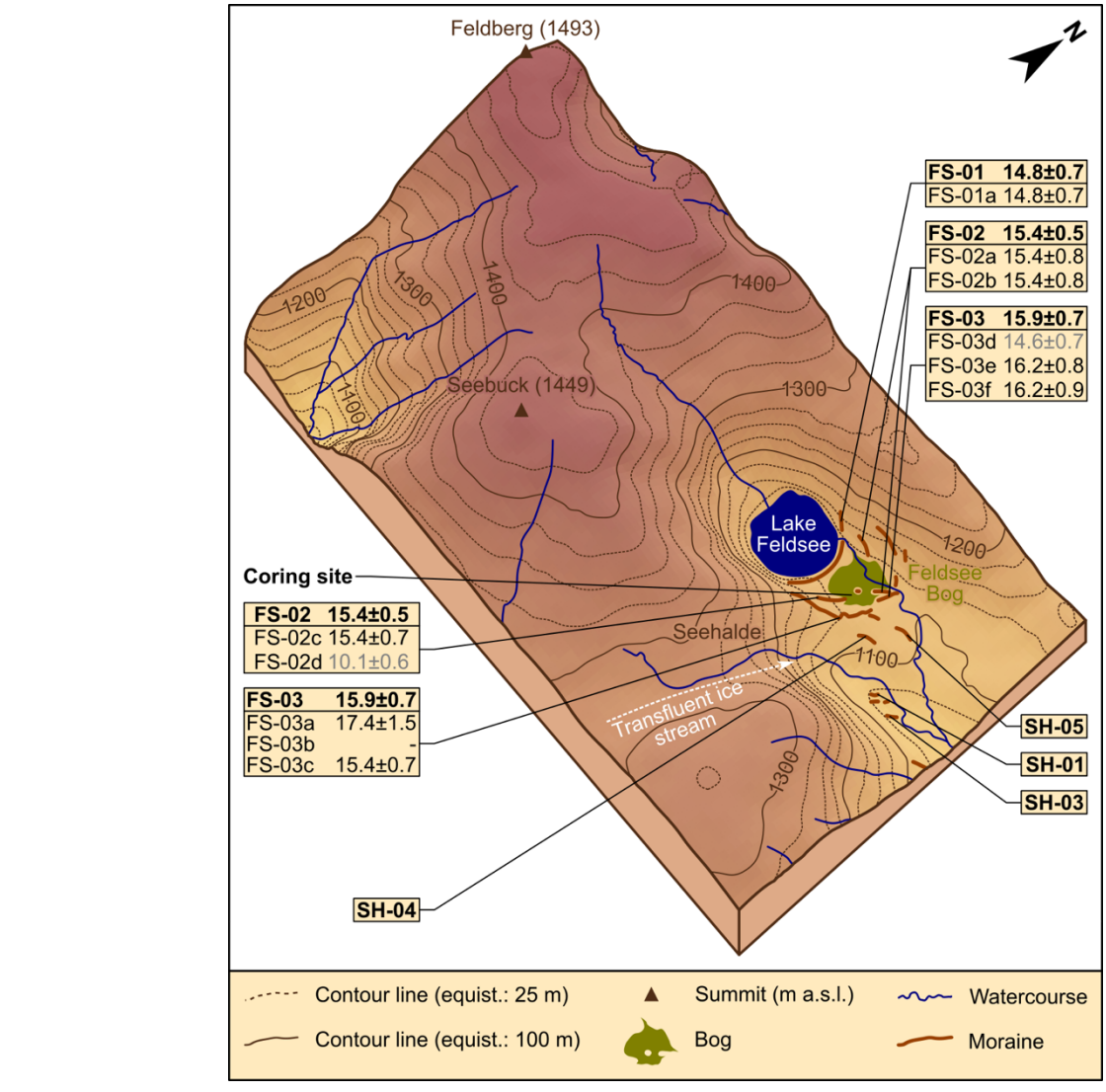

Figure 7: Map of moraines at the study site and the immediate surroundings. CRE ages and associated uncertainties (i.e., external uncertainties) of moraine boulders are given in ka before 2010 CE and ka, respectively. Bold ages are landform ages. Ages in grey were classified as outliers. See NASA Jet Propulsion Laboratory (2013) for a description of the DEM in the background.

The FS-02a, FS-02b, FS-02c and FS-02d boulders on the moraine at position FS-02 gave ages of 15.4±0.8 ka, 15.4±0.8 ka, 15.4±0.7 ka, and 10.1±0.6 ka, respectively. After the exclusion of the outlying age of the FS-02d boulder (10.1±0.6 ka), the remaining ages yielded a landform age of 15.4±0.5 ka. The only sufficiently large and stable boulder on the ice-marginal moraine at position FS-01 was exposure dated to 14.8±0.7 ka.

https://doi.org/10.5194/gchron-2023-27
Preprint. Discussion started: 9 January 2024

Overall, the presented ages are, apart from a few outliers, internally consistent, and the landform ages comply with the stratigraphy. With 15.4±0.8 ka, 15.4±0.8 ka, and 15.4±0.7 ka, the ages of the FS-02a, FS-02b, and FS-02c boulders on the moraine at position FS-02 are remarkably consistent (Reduced χ^2: 0.0).

6 Discussion

Determining the concentration of in situ accumulated cosmogenic ^{10}Be in boulders on moraines in the Feldsee Cirque and applying radiocarbon dating, tephrochronology, and luminescence dating to stratigraphically younger lake sediments allowed us to establish the internally robust BF production rate, the first ^{10}Be production rate for the mid-elevation Variscan mountain ranges of Central Europe. In Sect. 6.1, we discuss the robustness of this production rate. We then evaluate previously suggested corrections of CRE ages for postdepositional weathering (Sect. 6.2). In Sect. 6.3, we compare the local production rate with existing estimates for Europe. A detailed discussion of the implications of this study for the Late Pleistocene glacial history of the southern Black Forest would go beyond the scope of this paper and will be discussed in future work.

6.1 Robustness of the BF ^{10}Be production rate

The modelled basal age of the lake sediments above the moraine at the ice-marginal position FS-02 (mean age and 1σ uncertainty: 15630±450 cal. a BP) underpins the BF ^{10}Be production rate. Radiocarbon dating of macrofossils at decompacted depths of 5.61, 5.56, and 5.54 m resulted in consistent ages and, therefore, we regard the age-depth model as robust. In addition, IRSL dating of sediments at a decompacted depth of 5.51 m (FSM-5 sample) gave concordant ages of 14.0±1.2 ka and 15.8±1.7 ka, respectively.

The calibration of the BF ^{10}Be production rate was based on the implicit assumption that the macrofossils in the lake sediments provide a minimum age for both the moraines at positions FS-03 and FS-02. Due to the absence of a suitable record, such as a bog downstream of the moraines at position FS-03, we were unable to determine both the maximum ages of the landforms and the lowest possible production rate at the study site. Therefore, we conclude that the possible maximum production rate at the study site is relatively well constrained due to internally robust radiocarbon and luminescence ages, whereas we regard the lower limit of the production rate as less reliable due to the absence of information on the maximum age of the moraines at positions FS-03 and FS-02.

6.2 Evaluation of previously suggested corrections for snow shielding and postdepositional weathering

The “baseline” BF production rate offers the unique opportunity to assess previous corrections of CRE ages for postdepositional weathering and snow cover. In their studies on the Late Pleistocene glacial history of the southern Black Forest, Hofmann et al. (2022, 2023) calculated CRE ages with the Chironico landslide production rate. To account for the

https://doi.org/10.5194/gchron-2023-27
Preprint. Discussion started: 9 January 2024

stronger weathering and snow cover bias in their study areas, these authors corrected CRE ages for snow cover with a snow shielding factor (~0.974) deduced from meteorological data obtained between 1961 CE and 1990 CE at the weather station near Lake Titisee, located at about 850 m a.s.l. and about 10 km to the NE of the study area. These authors also corrected the ages for postdepositional weathering based on the weathering rate from the Bavarian Forest (0.24 cm ka^{-1}; based on Reuther, 2007). The corrections resulted in about 5% older CRE ages. It should be noted that their proposed corrections for postdepositional weathering and snow cover are technically wrong. Hofmann et al. (2022, 2023) essentially corrected their CRE ages twice for snow cover and postdepositional weathering, as the boulders at the Chironico landslide are affected by a snow cover and weathering bias. Irrespective of this discussion, their approach offered the opportunity to consider the stronger bias in their study areas.

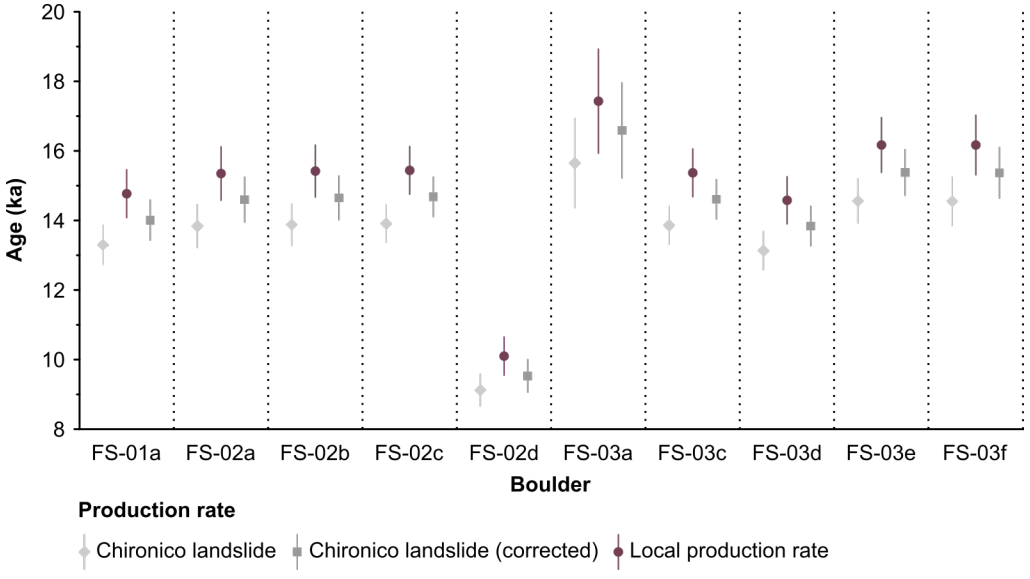

Figure 8: CRE ages of boulders and external CRE age uncertainties, calculated with the Chironico landslide production rate (Claude et al., 2014) and the BF production rate (this study).

Figure 8 shows the uncorrected and the corrected CRE ages for the study site, calculated with the Chironico landslide production rate. Most of the uncorrected ages calculated with this production rate at the overlap within 2σ uncertainties with the ages computed with the BF production rate. This broad agreement reinforces the hypothesis that CRE dating of moraine boulders is a suitable method for reconstructing the Late Pleistocene glacier variations in the mid-elevation Variscan mountain ranges of Central Europe. Figure 8 reveals that the corrected CRE ages align better with independent age control. Nevertheless, the ages calculated with the BF production rate are, on average, 5.3% older than the corrected ages, calculated with the Chironico landslide production rate. This offset underlines that CRE ages of moraine boulders strictly represent minimum ages for glacier recession from moraines.

https://doi.org/10.5194/gchron-2023-27
Preprint. Discussion started: 9 January 2024

Three possible explanations for the remaining offset of the ages appear possible: (i) We have corrected the ages sufficiently for snow cover and postdepositional weathering but have ignored other factors that do affect CRE ages, such as soil cover on the boulders at the study site. (ii) We might have simply corrected the ages insufficiently for snow cover and postdepositional weathering, and other factors do not play an important role. (iii) The correction for snow cover and postdepositional weathering was insufficient and we have ignored other important factors.

6.3 Comparison with previously published European production rates

We hereinafter discuss the BF ^{10}Be production rate for the southern Black Forest in the context of previously published European production rates (Table 9). Note that all SLHL production rates in CREp mentioned in the following paragraphs refer to time-dependent 'Lm' scaling (Nishiizumi et al., 1989; Lal, 1991; Stone, 2000; Balco et al., 2008), the ERA atmosphere model (Uppala et al., 2005), and the atmospheric ^{10}Be-based geomagnetic database (Muscheler et al., 2005).

Table 9: The BF local production rate and previously published European ^{10}Be production rates in CREp (Martin et al., 2017). We did not include the Rannoch Moor production rate, as this production rate is not commonly accepted (cf., Lowe et al., 2019, and references therein).

Reference site	Coordinates (WGS 1984 coordinate reference system)		Elevation (m a.s.l.)	Age (ka before 2010 CE)	Beryllium-10 production rate (atoms ^{10}Be g^{-1} quartz a^{-1} at SLHL)	Reference
	Latitude	Longitude				
Feldsee Cirque (Germany)	47.8706 °N	8.0375 °E	1107	15.63±0.45	3.66±0.12	This study
Chironico landslide (Switzerland)	46.4155 °N	8.8524 °E	761	13.38±0.11	4.10±0.10	Claude et al. (2014)
Mount Billingen 6 (Sweden)	58.5189 °N	13.7294 °E	119	11.53±0.11	4.32±0.18	Stroeven et al. (2015)
Mount Billingen 1 (Sweden)	58.5341 °N	13.7597 °E	95	10.73±0.35	4.14±0.30	
Mount Billingen 3 (Sweden)	58.5003 °N	13.6383 °E	106	11.11±0.20	4.25±0.30	
Halsnøy moraine (Norway)	59.7808 °N	5.79079 °E	77	11.64±0.10	4.43±0.08	Goehring et al. (2012)
Oldedalen rock avalanche (Norway)	61.6667 °N	6.8150 °E	127	6.06±0.11	4.23±0.14	
Grøtlandsura rock avalanche (Norway)	68.9112 °N	17.5224 °E	71	11.47±0.11	3.48±0.10	Fenton et al. (2011)
Russenes rock avalanche (Norway)	69.2135 °N	19.4731 °E	109	10.99±0.08	3.84±0.13	
Kyleakin Pass (Scotland)	57.2206 °N	5.7243 °W	309	11.75±0.30	4.46±0.26	Borchers et al. (2016)
Coire Mhic Fearchair (Scotland)	57.2408 °N	5.9727 °W	442		4.23±0.12	
Coire nan Arr (Scotland)	57.4141 °N	5.6438 °W	139		4.27±0.11	
Maol Chean Dearg (Scotland)	57.4874 °N	5.4493 °W	521		4.20±0.11	

https://doi.org/10.5194/gchron-2023-27
Preprint. Discussion started: 9 January 2024

The internally robust "baseline" BF ^{10}Be production rate (3.66±0.12 atoms ^{10}Be g^{-1} quartz a^{-1} at SLHL) does, apart from the production rates at the Russenes and Grøtlandsura rock avalanches (Fenton et al., 2011), not overlap at the 1σ level with other previously published production rates for Europe in CREp (Fig. 9). Most notably, the ^{10}Be production rate for the southern Black Forest is 10.7% and 10.9% lower than the only regional ^{10}Be production rate (Chironico landslide production rate; 4.10±0.10 atoms ^{10}Be g^{-1} quartz a^{-1} at SLHL) and the canonical global production rate in CREp (4.11±0.19 atoms ^{10}Be g^{-1} quartz a^{-1} at SLHL), respectively. However, the BF production rate overlaps with the Chironico landslide production rate, the global production rate, and several regional production rates at the 2σ level (Fig. 9).

https://doi.org/10.5194/gchron-2023-27
Preprint. Discussion started: 9 January 2024

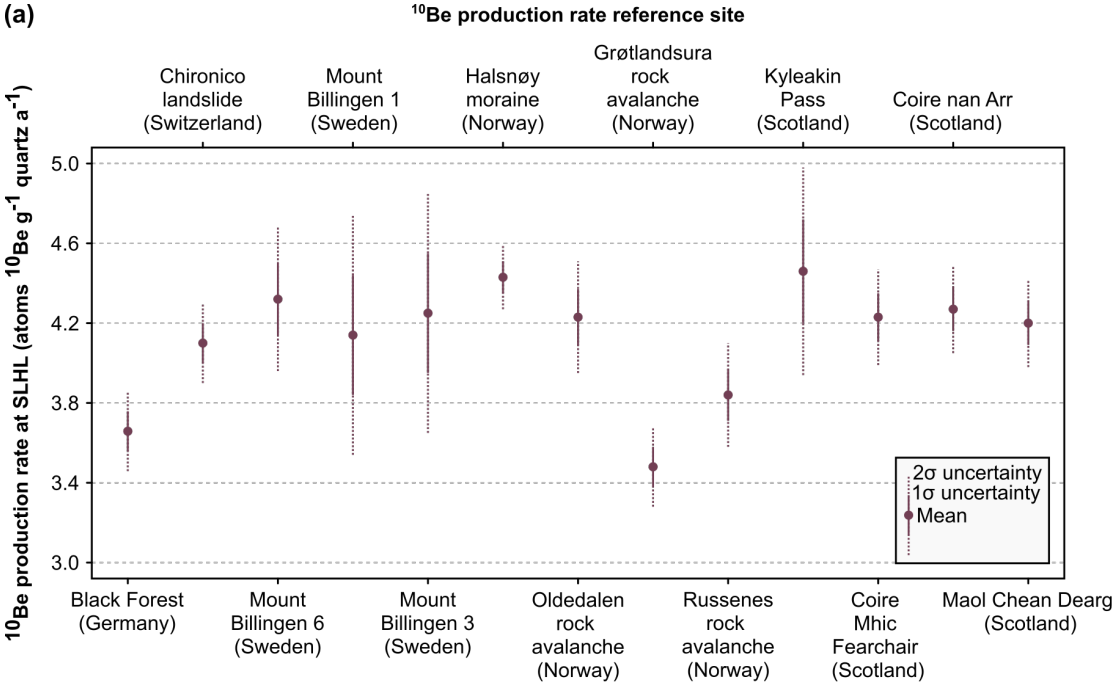

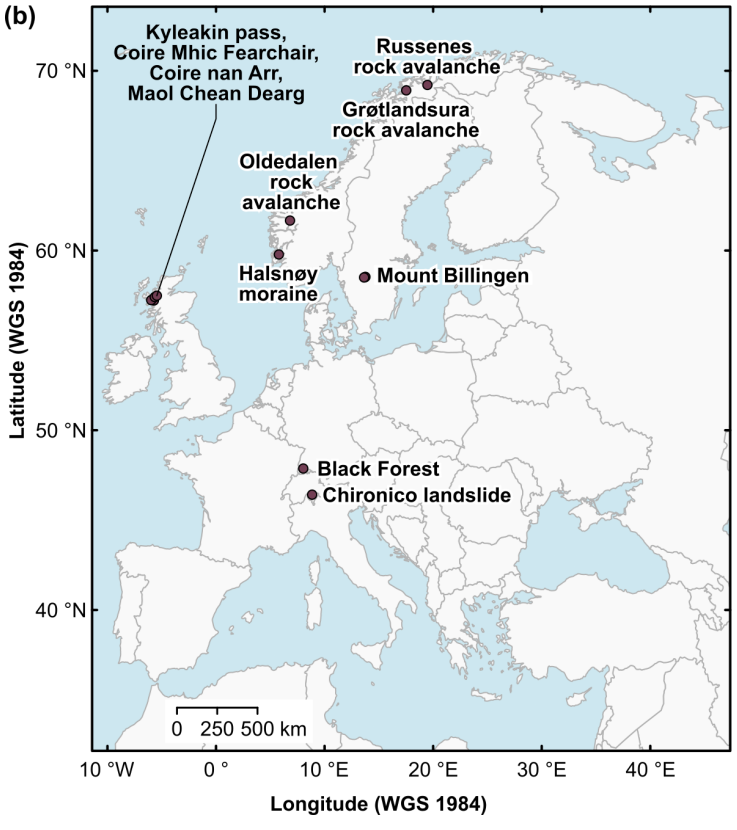

https://doi.org/10.5194/gchron-2023-27
Preprint. Discussion started: 9 January 2024

Figure 9: (a) European ^{10}Be production rates available in CREp (Martin et al., 2017). We did not include the Rannoch Moor ^{10}Be production rate in this compilation, as this production rate is not commonly accepted (cf., Lowe et al., 2019, and references therein). (b) Map of the production rate reference sites mentioned in panel (a).

6.4 Why is the presented local production rate lower than previous European production rates?

We argue that the agreement of the production rates at the 2σ level is due to (i) the comparably large scatter of production rates, since (ii) the Chironico landslide and the moraines at the Feldsee Bog have a similar age, and as (iii) the air pressure fields were probably similar at both the Feldsee Bog and the Chironico landslide during the exposure of the sampled boulders. But why do the production rates not agree at the 1σ level?

Overlapping production rates at the 1σ level would have additionally required that (i) changes in the geomagnetic field simultaneously affected both sites (ii) postdepositional weathering rates were similar at both sites, (iii) the snow cover on the sampling surfaces during winter was comparable, (iv) shielding by trees reduced the cosmic ray flux at both sites in a similar magnitude, and that (v) other factors, such as soil cover on sampling surfaces, played a similar role during the exposure of the boulders. Due to the comparably short distance between the Chironico landslide and the Feldsee Bog (~170 km), changes in the geomagnetic field probably do not account for the offset. The postdepositional weathering bias at the study site was probably stronger due to the presence of soils, mosses, and shrubs on most of the sampled boulders that slowed down the production rate (cf., Ahnert, 2009) and resulted in higher weathering rates (cf., Dunai, 2010). Unfortunately, we did not observe any protruding quartz veins on the sampled boulders that would have allowed for determining a site-specific rate of removal of rock due to weathering which would have then allowed for evaluating this hypothesis. The snow cover bias at the study site was probably stronger than at the Chironico landslide, as the Feldsee Bog is situated in a sheltered position, at a much higher elevation, and at a higher latitude. To the best knowledge of the authors, no data on the duration and thickness of the snow cover during winter is available from a weather station close to the Chironico landslide. We were thus unable to confirm this assumption with quantitative data. The sampled boulders at both the Feldsee Bog and the Chironico landslide were situated in forested areas and, thus, the forest canopy probably slowed down the effective production rates at both sites in a similar order of magnitude. As the landslide is located at both a lower latitude and elevation, the forest cover bias at the Chironico landslide should have been stronger. In contrast to the boulders at the study site, the boulders on the Chironico landslide sampled by Claude et al. (2014) were devoid of soil, mosses, and shrubs. We thus conclude that a stronger snow cover and postdepositional weathering bias in the study area, and the presence of soil, mosses, and shrubs on the boulders at the study site explain the relatively low BF production rate.

7 Conclusions

Applying a multi-method approach to ice-marginal moraines and stratigraphically younger lake sediments in the southern Black Forest yielded consistent geochronological data and allowed for deriving the BF ^{10}Be production rate, the first ^{10}Be

https://doi.org/10.5194/gchron-2023-27
Preprint. Discussion started: 9 January 2024

production rate for mid-elevation Variscan mountain ranges of central Europe. The resulting production rate turned out to be lower than most Europan production rates and about 12% lower than the canonical global ^{10}Be production rate. We attribute this offset to a strong influence of snow shielding, postdepositional weathering, and soil, moss, and shrub cover at the study site. Assessing a previously suggested correction for snow shielding and postdepositional weathering revealed that the correction might have been too weak. Future studies will have to reconcile existing CRE ages of moraine boulders in the mid-elevation mountain ranges in Central Europe with the presented local ^{10}Be production rate and to revise previous interpretations of the ages. At sites with a similar snow shielding, postdepositional weathering, and forest cover bias, ages will shift by more than 10%. The local ^{10}Be production rate presented here will have crucial implications for the Late Pleistocene glacial history of the formerly glaciated mid-elevation (Variscan) mountain ranges in Central Europe and for reconstructing past atmospheric circulation patterns over Europe.

The BF production rate will also be useful for future CRE dating studies in Central Europe and adjacent regions. It should be borne in mind that the "baseline" BF production rate should not be extrapolated to lowlands due to the comparably large snow shielding, weathering, and postdepositional weathering bias at the study site. With the data presented in this paper, researchers should decide on a site-by-site basis whether the "baseline", snow-cover-corrected, or the snow-cover- and postdepositional-weathering-corrected production rate is most appropriate. Due to a lower 1σ error (0.12-0.13 atoms ^{10}Be g^{-1} quartz a^{-1} at SLHL) than the 1σ uncertainty (0.19 atoms ^{10}Be g^{-1} quartz a^{-1} at SLHL) of the canonical global production rate in CREp, the application of the local production rates presented in this paper will allow for calculating more accurate CRE ages.

This study shows that luminescence dating is a useful complementary geochronological technique for the calibration of ^{10}Be production rates with independent radiocarbon ages. The local ^{10}Be production rate presented here does not only rely on one line of evidence, but on three independent dating methods. If these lines of evidence converge, a robust local ^{10}Be production rate can be derived with either radiocarbon ages or ages inferred from an age-depth model. Luminescence dating should, however, not take the place of radiocarbon dating, as the comparably large uncertainties of luminescence ages would translate into large errors of production rates.

Data availability

Watercourses and lakes in Fig. 7 are available at LUBW (2022a) and LUBW (2022b), respectively. The DEM in Figs. 1 and 7 (NASA Jet Propulsion Laboratory, 2013) is available for download in the Earth Explorer of the United States Geological Survey (USGS; https://earthexplorer.usgs.gov, last access: 5 December 2023). Meteorological data for the closest weather station to the study site are available at DWD (2023).

https://doi.org/10.5194/gchron-2023-27
Preprint. Discussion started: 9 January 2024

Team list

ASTER Team: Georges Aumaître, Karim Keddadouche, and Fawzi Zaidi

Author contribution

FP and FMH designed the study. FMH and AF undertook the fieldwork. FMH, CR, LG, MaS, MeS, AF, and LL conducted laboratory work. The ASTER Team performed the AMS measurements. FMH, CR, LG, MaS, MeS, AF, and FP processed and interpreted the data. FMH drafted the manuscript and the figures with contributions from FP, LG, and CR. All authors contributed to the final version of the manuscript.

Competing interests

The authors have declared that there are no competing interests.

Acknowledgements

We thank Florian Rauscher for his help during fieldwork and for his support during sample preparation for CRE dating. William McCreary III supported us during the coring campaign at the Feldsee Bog. The forestry department of the Breisgau-Hochschwarzwald district kindly provided a forest access permit. We thank the nature protection department of *Regierungspräsidium Freiburg* and the Feldberg Natural Reserve, particularly Clemens Glunk and Achim Laber, for the permission to sample moraine boulders for CRE dating. Matthias Geyer (Geotourist Freiburg) kindly provided the photo of the study site taken from a gilder. We thank the State Geological Survey of Baden-Württemberg (LRGB) for providing LiDAR data of the Baden-Württemberg State Agency for Spatial Information and Rural Development (LGL) in a collaborative way.

Financial support

This research was undertaken while Felix Martin Hofmann was in receipt of a PhD studentship of *Studienstiftung des Deutschen Volkes*. This study was financially supported by the German Research Foundation (DFG) through the 'Geometry, chronology and dynamics of the last Pleistocene glaciation of the Black Forest', 'Chronology of the glaciation of the southern Black Forest after the Late Pleistocene glaciation maximum', and 'Gerät für Lumineszenz-Messungen und Datierungen' projects granted to FP (project numbers: 426333515, 516126018, and 282256512, respectively). The French AMS national facility ASTER at CEREGE is supported by the INSU/CNRS, the ANR through the 'Projets thématiques d'excellence' programme for the 'Equipements d'excellence' ASTER-CEREGE action and IRD.

https://doi.org/10.5194/gchron-2023-27
Preprint. Discussion started: 9 January 2024

References

Ahnert, F.: Einführung in die Geomorphologie, 4. Aufl., Ulmer, Stuttgart, 393 pp., 2009.

Amschwand, D., Ivy-Ochs, S., Frehner, M., Steinemann, O., Christl, M., and Vockenhuber, C.: Deciphering the evolution of the Bleis Marscha rock glacier (Val d'Err, eastern Switzerland) with cosmogenic nuclide exposure dating, aerial image correlation, and finite element modeling, The Cryosphere, 15, 2057–2081, https://doi.org/10.5194/tc-15-2057-2021, 2021.

Andrieu, V., Beaulieu, J.-L., Ponel, P., and Reille, M.: [Les distorsions de l'enregistrement pollinique de l'histoire de la végétation du dernier cycle climatique: Exemples de séquences lacustres du Sud de la France]. Distorsions in the pollen record of vegetation history over the last climatic cycle: examples of lake sequences from southern France, Geobios, 30, 195–202, https://doi.org/10.1016/S0016-6995(97)80091-5, 1997.

Arnold, M., Aumaître, G., Bourlès, D. L., Keddadouche, K., Braucher, R., Finkel, R. C., Nottoli, E., Benedetti, L., and Merchel, S.: The French accelerator mass spectrometry facility ASTER after 4 years: Status and recent developments on ^{36}Cl and ^{129}I, Nucl. Instrum. Meth. B, 294, 24–28, https://doi.org/10.1016/j.nimb.2012.01.049, 2013.

Arnold, M., Merchel, S., Bourlès, D. L., Braucher, R., Benedetti, L., Finkel, R. C., Aumaître, G., Gottdang, A., and Klein, M.: The French accelerator mass spectrometry facility ASTER: Improved performance and developments, Nucl. Instrum. Meth. B, 268, 1954–1959, https://doi.org/10.1016/j.nimb.2010.02.107, 2010.

Balco, G.: Documentation—v3 exposure age calculator. Ancillary calculations and plots., https://sites.google.com/a/bgc.org/v3docs/documentation-v3-exposure-age-calculator/4-ancillary-calculations-and-plots, last access: 19 October 2023, 2023.

Balco, G.: Contributions and unrealized potential contributions of cosmogenic-nuclide exposure dating to glacier chronology, 1990–2010, Quaternary Sci. Rev., 30, 3–27, https://doi.org/10.1016/j.quascirev.2010.11.003, 2011.

Balco, G., Stone, J. O., Lifton, N. A., and Dunai, T. J.: A complete and easily accessible means of calculating surface exposure ages or erosion rates from ^{10}Be and ^{26}Al measurements, Quat. Geochronol., 3, 174–195, https://doi.org/10.1016/j.quageo.2007.12.001, 2008.

Borchers, B., Marrero, S., Balco, G., Caffee, M., Goehring, B., Lifton, N., Nishiizumi, K., Phillips, F., Schaefer, J., and Stone, J.: Geological calibration of spallation production rates in the CRONUS-Earth project, Quat. Geochronol., 31, 188–198, https://doi.org/10.1016/j.quageo.2015.01.009, 2016.

Boxleitner, M., Ivy-Ochs, S., Egli, M., Brandova, D., Christl, M., and Maisch, M.: Lateglacial and Early Holocene glacier stages - New dating evidence from the Meiental in central Switzerland, Geomorphology, 340, 15–31, https://doi.org/10.1016/j.geomorph.2019.04.004, 2019.

Braucher, R., Guillou, V., Bourlès, D. L., Arnold, M., Aumaître, G., Keddadouche, K., and Nottoli, E.: Preparation of ASTER in-house ^{10}Be/^{9}Be standard solutions, Nucl. Instrum. Meth. B, 361, 335–340, https://doi.org/10.1016/j.nimb.2015.06.012, 2015.

https://doi.org/10.5194/gchron-2023-27
Preprint. Discussion started: 9 January 2024

Bronk Ramsey, C.: Bayesian Analysis of Radiocarbon Dates, Radiocarbon, 51, 337–360, https://doi.org/10.1017/S0033822200033865, 2009.

Bronk Ramsey, C.: Deposition models for chronological records, Quaternary Sci. Rev., 27, 42–60, https://doi.org/10.1016/j.quascirev.2007.01.019, 2008.

Bronk Ramsey, C. and Lee, S.: Recent and Planned Developments of the Program OxCal, Radiocarbon, 55, 720–730, https://doi.org/10.1017/S0033822200057878, 2013.

Chmeleff, J., Blanckenburg, F. von, Kossert, K., and Jakob, D.: Determination of the ^{10}Be half-life by multicollector ICP-MS and liquid scintillation counting, Nucl. Instrum. Meth. B, 268, 192–199, https://doi.org/10.1016/j.nimb.2009.09.012, 2010.

Claude, A., Ivy-Ochs, S., Kober, F., Antognini, M., Salcher, B., and Kubik, P. W.: The Chironico landslide (Valle Leventina, southern Swiss Alps): age and evolution, Swiss J. Geosci., 107, 273–291, https://doi.org/10.1007/s00015-014-0170-z, 2014.

Dawson, A. G., Bishop, P., Hansom, J., and Fabel, D.: ^{10}Be exposure age dating of Late Quaternary relative sea level changes and deglaciation of W Jura and NE Islay, Scottish Inner Hebrides, Earth Env. Sci. T. R. So., 113, 253–266, https://doi.org/10.1017/S175569102200010X, 2022.

Degering, D. and Degering, A.: Change is the only constant - time-dependent dose rates in luminescence dating, Quat. Geochronol., 58, 101074, https://doi.org/10.1016/j.quageo.2020.101074, 2020.

Dunai, T.: Cosmogenic nuclides: Principles, concepts and applications in the earth surface sciences, Cambridge University Press, Cambridge, 187 pp., 2010.

DWD: Open Data [data set], https://opendata.dwd.de, 2023.

Ehlers, J., Gibbard, P. L., and Hughes, P. D. (Eds.): Quaternary Glaciations - Extent and Chronology.: A Closer Look, Developments in Quaternary Sciences, 15, Elsevier, Amsterdam, Oxford, 2011.

Erb, L.: Die Geologie des Feldbergs, in: Der Feldberg im Schwarzwald, edited by: Müller, K., L. Bielefelds Verlag KG, Freiburg i. Br., 22–96, 1948.

Fenton, C. R., Hermanns, R. L., Blikra, L. H., Kubik, P. W., Bryant, C., Niedermann, S., Meixner, A., and Goethals, M. M.: Regional ^{10}Be production rate calibration for the past 12 ka deduced from the radiocarbon-dated Grøtlandsura and Russenes rock avalanches at 69° N, Norway, Quat. Geochronol., 6, 437–452, https://doi.org/10.1016/j.quageo.2011.04.005, 2011.

Gaar, D., Graf, H. R., and Preusser, F.: New chronological constraints on the timing of Late Pleistocene glacier advances in northern Switzerland, E&G Quaternary Sci. J., 68, 53–73, https://doi.org/10.5194/egqsj-68-53-2019, 2019.

Galbraith, R. F. and Roberts, R. G.: Statistical aspects of equivalent dose and error calculation and display in OSL dating: An overview and some recommendations, Quat. Geochronol., 11, 1–27, https://doi.org/10.1016/j.quageo.2012.04.020, 2012.

Gegg, L. and Gegg, J.: Poor Man's Line Scan – a simple tool for the acquisition of high-resolution, undistorted drill core photos, Scientific Drilling, 32, 55–59, https://doi.org/10.5194/sd-32-55-2023, 2023.

https://doi.org/10.5194/gchron-2023-27
Preprint. Discussion started: 9 January 2024

Geyer, O. F. and Gwinner, M. P.: Geologie von Baden-Württemberg, 5th ed., Geyer, M. and Nitsch, E. (Eds.), Schweizerbart, Stuttgart, 627 pp., 2011.

Glew, J. R., Smol, J. P., and Last, W. M.: Sediment Core Collection and Extrusion, in: Tracking Environmental Change Using Lake Sediments: Basin Analysis, Coring, and Chronological Techniques, edited by: Last, W. M. and Smol, J. P., Springer Netherlands, Dordrecht, 73–105, https://doi.org/10.1007/0-306-47669-X_5, 2001.

Goehring, B. M., Lohne, Ø. S., Mangerud, J., Svendsen, J. I., Gyllencreutz, R., Schaefer, J., and Finkel, R.: Late glacial and holocene ^{10}Be production rates for western Norway, J. Quaternary Sci., 27, 89–96, https://doi.org/10.1002/jqs.1517, 2012.

Gosse, J. C. and Phillips, F. M.: Terrestrial in situ cosmogenic nuclides: theory and application, Quaternary Sci. Rev., 20, 1475–1560, https://doi.org/10.1016/S0277-3791(00)00171-2, 2001.

Hall, K., Thorn, C., and Sumner, P.: On the persistence of 'weathering', Geomorphology, 149-150, 1-10, https://doi.org/10.1016/j.geomorph.2011.12.024, 2012.

Heiri, O., Koinig, K. A., Spötl, C., Barrett, S., Brauer, A., Drescher-Schneider, R., Gaar, D., Ivy-Ochs, S., Kerschner, H., Luetscher, M., Moran, A., Nicolussi, K., Preusser, F., Schmidt, R., Schoeneich, P., Schwörer, C., Sprafke, T., Terhorst, B., and Tinner, W.: Palaeoclimate records 60–8 ka in the Austrian and Swiss Alps and their forelands, Quaternary Sci. Rev., 106, 186–205, https://doi.org/10.1016/j.quascirev.2014.05.021, 2014.

Heiri, O., Lotter, A. F., and Lemcke, G.: Loss on ignition as a method for estimating organic and carbonate content in sediments: reproducibility and comparability of results, Journal of Paleolimnology, 25, 101–110, https://doi.org/10.1023/A:1008119611481, 2001.

Hemmerle, H., May, J.-H., and Preusser, F.: Übersicht über die pleistozänen Vergletscherungen des Schwarzwaldes, Ber. Naturf. Ges. Freiburg i. Br., 106, 31–67, 2016.

Hilger, P., Hermanns, R. L., Gosse, J. C., Jacobs, B., Etzelmüller, B., and Krautblatter, M.: Multiple rock-slope failures from Mannen in Romsdal Valley, western Norway, revealed from Quaternary geological mapping and ^{10}Be exposure dating, Holocene, 28, 1841–1854, https://doi.org/10.1177/0959683618798165, 2018.

Hofmann, F. M., Rauscher, F., McCreary, W., Bischoff, J. P., and Preusser, F.: Revisiting Late Pleistocene glacier dynamics north-west of the Feldberg, southern Black Forest, Germany, E&G Quaternary Sci. J., 69, 61–87, https://doi.org/10.5194/egqsj-69-61-2020, 2020.

Hofmann, F. M.: Geometry, chronology and dynamics of the last Pleistocene glaciation of the Black Forest, E&G Quaternary Sci. J., 72, 235–237, https://doi.org/10.5194/egqsj-72-235-2023, 2023.

Hofmann, F. M.: Technical note: Evaluating a geographical information system (GIS)-based approach for determining topographic shielding factors in cosmic-ray exposure dating, Geochronology, 4, 691–712, https://doi.org/10.5194/gchron-4-691-2022, 2022.

https://doi.org/10.5194/gchron-2023-27
Preprint. Discussion started: 9 January 2024

Hofmann, F. M. and Konold, W.: [Landschaftsgeschichte des oberen Seebachtals, Südschwarzwald (Exkursion D am 14. September 2023)]. Landscape history of the upper Seebachtal, southern Black Forest, Germany, Jber. Mitt. oberrhein. geol. Ver., 105, 63–89, https://doi.org/10.1127/jmogv/105/0004, 2023.

Hofmann, F. M., Groos, A. R., Garcia Morabito, E., Struck, J., Gnägi, C., Scharf, A., Rugel, G., Merchel, S., and Zech, R.: A regional assessment of the deglaciation history of the Swiss Plateau based on newly obtained and re-evaluated Be-10 cosmic-ray exposure ages, Quaternary Sci. Adv., 13, 100124, https://doi.org/10.1016/j.qsa.2023.100124, 2024.

Hofmann, F. M., Steiner, M., Hergarten, S., ASTER Team, and Preusser, F.: Limitations of precipitation reconstructions using equilibrium line altitudes exemplified for former glaciers in the Southern Black Forest, Central Europe, Quaternary Res., 1-25, https://doi.org/10.1017/qua.2023.53, 2023.

Hofmann, F. M., Preusser, F., Schimmelpfennig, I., Léanni, L., and ASTER Team: Late Pleistocene glaciation history of the southern Black Forest, Germany: ^{10}Be cosmic-ray exposure dating and equilibrium line altitude reconstructions in Sankt Wilhelmer Tal, J. Quaternary Sci., 37, 688–706, https://doi.org/10.1002/jqs.3407, 2022.

Huntley, D. J. and Baril, M. R.: The K content of the K-feldspars being measured in optical dating or in thermoluminescence dating, Ancient TL, 15, 11–13, 1997.

Ivanovich, M. and Harmon, R. S.: Uranium-series disequilibrium: applications to earth, marine, and environmental sciences, 2nd edition, Clarendon Press, Oxford (United Kingdom), 1992.

Ivy-Ochs, S. and Kober, F.: Surface exposure dating with cosmogenic nuclides, E&G Quaternary Sci. J., 57, 179–209, https://doi.org/10.3285/eg.57.1-2.7, 2008.

Ivy-Ochs, S., Kerschner, H., and Schlüchter, C.: Cosmogenic nuclides and the dating of Lateglacial and Early Holocene glacier variations: The Alpine perspective, Quat. Intern., 164-165, 53–63, https://doi.org/10.1016/j.quaint.2006.12.008, 2007.

Korschinek, G., Bergmaier, A., Faestermann, T., Gerstmann, U. C., Knie, K., Rugel, G., Wallner, A., Dillmann, I., Dollinger, G., Gostomski, C. L. von, Kossert, K., Maiti, M., Poutivtsev, M., and Remmert, A.: A new value for the half-life of ^{10}Be by Heavy-Ion Elastic Recoil Detection and liquid scintillation counting, Nucl. Instrum. Meth. B, 268, 187–191, https://doi.org/10.1016/j.nimb.2009.09.020, 2010.

Lal, D.: Cosmic ray labeling of erosion surfaces: in situ nuclide production rates and erosion models, Earth Planet. Sc. Lett., 104, 424–439, https://doi.org/10.1016/0012-821X(91)90220-C, 1991.

Lang, G.: Late-glacial fluctuations of timberline in the Black Forest (SW Germany), Veget. Hist. Archaeobot, 15, 373–375, https://doi.org/10.1007/s00334-006-0048-8, 2006.

Lang, G.: Seen und Moore des Schwarzwaldes als Zeugen spätglazialen und holozänen Vegetationswandels. Stratigraphische, pollenanalytische und großrestanalytische Untersuchungen., Andrias 16, Karlsruhe, 160 pp., 2005.

Lang, G., Merkt, J., and Streif, H.: Spätglazialer Gletscherrückzug und See- und Moorentwicklung im Südschwarzwald, Südwestdeutschland, Diss. Bot., 72 (Festschrift Welten), 213–234, 1984.

https://doi.org/10.5194/gchron-2023-27
Preprint. Discussion started: 9 January 2024

Le Roy, M., Deline, P., Carcaillet, J., Schimmelpfennig, I., Ermini, M., and ASTER Team: ^{10}Be exposure dating of the timing of Neoglacial glacier advances in the Ecrins-Pelvoux massif, southern French Alps, Quaternary Sci. Rev., 178, 118–138, https://doi.org/10.1016/j.quascirev.2017.10.010, 2017.

LGL (Landesamt für Geoinformation und Landentwicklung Baden-Württemberg): DGM aus ALS_1 [data set], https://www.lgl-bw.de/Produkte/Geodaten/Digitale-Gelaendemodelle, 2015.

LGRB (Landesamt für Geologie, Rohstoffe und Bergbau Baden-Württemberg): Das Feldseekar, https://lgrbwissen.lgrbbw.de/geotourismus/glazialformen/schwarzwald/feldseekar, last access: 18 April 2023, 2023.

LGRB: Geologische Karte von Baden-Württemberg 1 50 000 (GeoLa), https://produkte.lgrb-bw.de/catalog/list/?wm_group_id=15111, last access: 31 March 2023, 2013.

Li, Y.-K.: Determining topographic shielding from digital elevation models for cosmogenic nuclide analysis: a GIS model for discrete sample sites, J. Mt. Sci., 15, 939–947, https://doi.org/10.1007/s11629-018-4895-4, 2018.

Liehl, E.: Landschaftsgeschichte des Feldberggebietes, in: Der Feldberg im Schwarzwald: subalpine Insel im Mittelgebirge, edited by: Landesanstalt für Umweltschutz Baden-Württemberg Institut für Ökologie und Naturschutz, Karlsruhe, 1982.

Lifton, N., Sato, T., and Dunai, T. J.: Scaling in situ cosmogenic nuclide production rates using analytical approximations to atmospheric cosmic-ray fluxes, Earth Planet. Sc. Lett., 386, 149–160, https://doi.org/10.1016/j.epsl.2013.10.052, 2014.

Lowe, J., Matthews, I., Mayfield, R., Lincoln, P., Palmer, A., Staff, R., and Timms, R.: On the timing of retreat of the Loch Lomond ('Younger Dryas') Readvance icefield in the SW Scottish Highlands and its wider significance, Quaternary Sci. Rev., 219, 171–186, https://doi.org/10.1016/j.quascirev.2019.06.034, 2019.

LUBW (Landesanstalt für Umwelt Baden-Württemberg): Fließgewässer (AWGN) [data set], https://rips-datenlink.lubw.de/UDO_download/Fliessgewaessernetz.zip, 2022a.

LUBW: Stehendes Gewässer (AWGN) [data set], https://rips-datenlink.lubw.de/UDO_download/StehendeGewaesser.zip, 2022b.

LUBW: Feldseemoor, http://www2.lubw.baden-wuerttemberg.de/public/abt2/dokablage/oac_77/moore01/405.htm, last access: 17 October 2023, 2006.

Martin, L. C. P., Blard, P. H., Balco, G., Lavé, J., Delunel, R., Lifton, N., and Laurent, V.: The CREp program and the ICE-D production rate calibration database: A fully parameterizable and updated online tool to compute cosmic-ray exposure ages, Quat. Geochronol., 38, 25–49, https://doi.org/10.1016/j.quageo.2016.11.006, 2017.

Masarik, J. and Wieler, R.: Production rates of cosmogenic nuclides in boulders, Earth Planet. Sc. Lett., 216, 201–208, https://doi.org/10.1016/S0012-821X(03)00476-X, 2003.

Matzarakis, A.: Klima, in: Der Feldberg: subalpine Insel im Schwarzwald, edited by: Regierungspräsidium Freiburg, Jan Thorbecke Verlag der Schwabenverlag AG, Ostfildern, 95–106, 2012.

Meinig, R.: [Halte und Eisrandbildungen des würmzeitlichen Bärental-Gletschers, Südschwarzwald]. Halts and ice margin formations of the Bärental-Glacier, southern Black Forest, in: [Spät- und postglaziale Gletscherschwankungen: Glazial-

https://doi.org/10.5194/gchron-2023-27
Preprint. Discussion started: 9 January 2024

und Periglazialformen]. Late- and postglacial oscillations of glaciers: glacial and periglacial landforms, Trier, 1980, 257–282, 1980.

Mentlík, P., Engel, Z., Braucher, R., and Léanni, L.: Chronology of the Late Weichselian glaciation in the Bohemian Forest in Central Europe, Quaternary Sci. Rev., 65, 120–128, https://doi.org/10.1016/j.quascirev.2013.01.020, 2013.

Mercier, J.-L., Kalvoda, J., Bourlès, D. L., Braucher, R., and Engel, Z.: Preliminary results of ^{10}Be dating of glacial landscape in the Giant Mountains, Acta Universitatis Carolinae Geographica, Supplementum, 35, 157–170, 2000.

Mercier, J.-L., Bourlès, D. L., Kalvoda, J., Braucher, R., and Paschen, A.: Deglaciation of the Vosges dated using ^{10}Be, Acta Universitatis Carolinae Geographica, 2, 139–155, 1999.

Metz, B.: Geomorphologische Karte 1:25 000 der Bundesrepublik Deutschland. GMK 25 Blatt 21. 8114 Feldberg, Geo Center, Stuttgart, 1985.

Metz, B. and Saurer, H.: Geomorphologie und Landschaftsentwicklung, in: Der Feldberg: subalpine Insel im Schwarzwald, edited by: Regierungspräsidium Freiburg, Jan Thorbecke Verlag der Schwabenverlag AG, Ostfildern, 14–62, 2012.

Millard, A. R.: Conventions for Reporting Radiocarbon Determinations, Radiocarbon, 56, 555–559, https://doi.org/10.2458/56.17455, 2014.

Muscheler, R., Beer, J., Kubik, P. W., and Synal, H. A.: Geomagnetic field intensity during the last 60,000 years based on ^{10}Be and ^{36}Cl from the Summit ice cores and ^{14}C, Quaternary Sci. Rev., 24, 1849–1860, https://doi.org/10.1016/j.quascirev.2005.01.012, 2005.

NASA Jet Propulsion Laboratory: NASA Shuttle Radar Topography Mission Global 1 arc second [data set], https://doi.org/10.5067/MEaSUREs/SRTM/SRTMGL1.003, 2013.

Nishiizumi, K., Winterer, E. L., Kohl, C. P., Klein, J., Middleton, R., Lal, D., and Arnold, J. R.: Cosmic ray production rates of ^{10}Be and ^{26}Al in quartz from glacially polished rocks, J. Geophys Res.-Sol. Ea., 94, 17907–17915, https://doi.org/10.1029/JB094iB12p17907, 1989.

Plug, L. J., Gosse, J. C., McIntosh, J. J., and Bigley, R.: Attenuation of cosmic ray flux in temperate forest, J. Geophys. Res., 112, https://doi.org/10.1029/2006JF000668, 2007.

Preusser, F. and Degering, D.: Luminescence dating of the Niederweningen mammoth site, Switzerland, Quat. Intern., 164-165, 106–112, https://doi.org/10.1016/j.quaint.2006.12.002, 2007.

Preusser, F., Degering, D., Fülling, A., and Miocic, J.: Complex Dose Rate Calculations in Luminescence Dating of Lacustrine and Palustrine Sediments from Niederweningen, Northern Switzerland, Geochronometria, 50, 28–49, https://doi.org/10.2478/geochr-2023-0003, 2023.

Preusser, F., Büschelberger, M., Kemna, H. A., Miocic, J., Mueller, D., and May, J.-H.: Exploring possible links between Quaternary aggradation in the Upper Rhine Graben and the glaciation history of northern Switzerland, Int. J. Earth Sci., 110, 1827–1846, https://doi.org/10.1007/s00531-021-02043-7, 2021.

https://doi.org/10.5194/gchron-2023-27
Preprint. Discussion started: 9 January 2024

Preusser, F., May, J.-H., Eschbach, D., Trauerstein, M., and Schmitt, L.: Infrared stimulated luminescence dating of 19th century fluvial deposits from the upper Rhine River, Geochronometria, 43, 131–142, https://doi.org/10.1515/geochr-2015-0045, 2016.

Preusser, F., Ramseyer, K., and Schlüchter, C.: Characterisation of low OSL intensity quartz from the New Zealand Alps, Rad. Meas., 41, 871–877, https://doi.org/10.1016/j.radmeas.2006.04.019, 2006.

Protin, M., Schimmelpfennig, I., Mugnier, J.-L., Ravanel, L., Le Roy, M., Deline, P., Favier, V., Buoncristiani, J.-F., Aumaître, G., Bourlès, D. L., and Keddadouche, K.: Climatic reconstruction for the Younger Dryas/Early Holocene transition and the Little Ice Age based on paleo-extents of Argentière glacier (French Alps), Quaternary Sci. Rev., 221, 105863, https://doi.org/10.1016/j.quascirev.2019.105863, 2019.

Ramsay, A. C.: On the Glacial Origin of certain Lakes in Switzerland, the Black Forest, Great Britain, Sweden, North America, and elsewhere, Quaterly Journal of the Geological Society of London, 18, 185–204, 1862.

Reimer, P. J., Austin, W. E. N., Bard, E., Bayliss, A., Blackwell, P. G., Bronk Ramsey, C., Butzin, M., Cheng, H., Edwards, R. L., Friedrich, M., Grootes, P. M., Guilderson, T. P., Hajdas, I., Heaton, T. J., Hogg, A. G., Hughen, K. A., Kromer, B., Manning, S. W., Muscheler, R., Palmer, J. G., Pearson, C., van der Plicht, J., Reimer, R. W., Richards, D. A., Scott, E. M., Southon, J. R., Turney, C. S. M., Wacker, L., Adolphi, F., Büntgen, U., Capano, M., Fahrni, S. M., Fogtmann-Schulz, A., Friedrich, R., Köhler, P., Kudsk, S., Miyake, F., Olsen, J., Reinig, F., Sakamoto, M., Sookdeo, A., and Talamo, S.: The IntCal20 Northern Hemisphere Radiocarbon Age Calibration Curve (0–55 cal kBP), Radiocarbon, 62, 725–757, https://doi.org/10.1017/RDC.2020.41, 2020.

Reinig, F., Wacker, L., Jöris, O., Oppenheimer, C., Guidobaldi, G., Nievergelt, D., Adolphi, F., Cherubini, P., Engels, S., Esper, J., Land, A., Lane, C., Pfanz, H., Remmele, S., Sigl, M., Sookdeo, A., and Büntgen, U.: Precise date for the Laacher See eruption synchronizes the Younger Dryas, Nature, 595, 66–69, https://doi.org/10.1038/s41586-021-03608-x, 2021.

Reuther, A. U.: Surface exposure dating of glacial deposits from the last glacial cycle. Evidence from the Eastern Alps, the Bavarian Forest, the Southern Carpathians and the Altai Mountains, Relief, Boden, Paläoklima, 21, Borntraeger, Berlin, Stuttgart, 213 pp., 2007.

Richter, D., Richter, A., and Dornich, K.: Lexsyg — A new system for luminescence research, Geochronometria, 40, 220–228, https://doi.org/10.2478/s13386-013-0110-0, 2013.

Ross, S.: Peirce's criterion for the elimination of suspect experimental data, J. Eng. Technol., 20, 1–12, 2003.

Schlüchter, C.: Sedimente des Gletschers (Teil I), Bulletin für angewandte Geologie, 2, 99–112, 1997.

Schoch-Baumann, A., Blöthe, J. H., Munack, H., Hornung, J., Codilean, A. T., Fülöp, R.-H., Wilcken, K., and Schrott, L.: Postglacial outsize fan formation in the Upper Rhone valley, Switzerland – gradual or catastrophic? Earth Surf. Proc. Land. 47, 1032–1053, https://doi.org/10.1002/esp.5301, 2022.

https://doi.org/10.5194/gchron-2023-27
Preprint. Discussion started: 9 January 2024

Schreiner, A.: Quartär, in: Geologische Karte 1:25 000 von Baden-Württemberg. Erläuterungen zu Blatt 8114 Feldberg, 2nd ed., edited by: Geologisches Landesamt Baden-Württemberg, Landesvermessungsamt Baden-Württemberg, Stuttgart, 67–95, 1990.

Schrepfer, H.: Zur Kenntnis der Eiszeit im Wutachgebiet, Mitt. bad. Landesver. Naturkunde u. Naturschutz, 1, 469–473, 1925.

Steinmann, G.: Die Bildungen der letzten Eiszeit im Bereiche des alten Wutachgebiets, Ber. oberrh. geol. Ver., 35, 16-23, 1902.

Stojakowits, P., Friedmann, A., and Bull, A.: Die spätglaziale Vegetationsgeschichte im oberen Illergebiet (Allgäu/Bayern), E&G Quaternary Sci. J., 63, 130–142, https://doi.org/10.3285/eg.63.2.02, 2014.

Stone, J. O.: Air pressure and cosmogenic isotope production, J. Geophys Res.-Sol. Ea., 105, 23753–23759, https://doi.org/10.1029/2000JB900181, 2000.

Stroeven, A. P., Heyman, J., Fabel, D., Björck, S., Caffee, M. W., Fredin, O., and Harbor, J. M.: A new Scandinavian reference ^{10}Be production rate, Quat. Geochronol., 29, 104–115, https://doi.org/10.1016/j.quageo.2015.06.011, 2015.

Stuart, F. M. and Dunai, T. J.: Advances in cosmogenic isotope research from CRONUS-EU, Quat. Geochronol., 4, 435–436, https://doi.org/10.1016/j.quageo.2009.09.009, 2009.

Uppala, S. M., Kållberg, P. W., Simmons, A. J., Andrae, U., Da Bechtold, V. C., Fiorino, M., Gibson, J. K., Haseler, J., Hernandez, A., Kelly, G. A., Li, X., Onogi, K., Saarinen, S., Sokka, N., Allan, R. P., Andersson, E., Arpe, K., Balmaseda, M. A., Beljaars, A. C. M., van Berg, L. de, Bidlot, J., Bormann, N., Caires, S., Chevallier, F., Dethof, A., Dragosavac, M., Fisher, M., Fuentes, M., Hagemann, S., Hólm, E., Hoskins, B. J., Isaksen, L., Janssen, P. A. E. M., Jenne, R., McNally, A. P., Mahfouf, J. F., Morcrette, J. J., Rayner, N. A., Saunders, R. W., Simon, P., Sterl, A., Trenberth, K. E., Untch, A., Vasiljevic, D., Viterbo, P., and Woollen, J.: The ERA-40 re-analysis, Q. J. Roy. Meteor. Soc., 131, 2961–3012, https://doi.org/10.1256/qj.04.176, 2005.

Vočadlová, K., Petr, L., Žáčková, P., Křížek, M., Křížová, L., Hutchinson, S. M., and Šobr, M.: The Lateglacial and Holocene in Central Europe: a multi-proxy environmental record from the Bohemian Forest, Czech Republic, Boreas, 44, 769–784, https://doi.org/10.1111/bor.12126, 2015.

Walchner, F. A.: Handbuch der Geognosie zum Gebrauche bei seinen Vorlesungen und zum Selbststudium mit besonderer Berücksichtigung der geognostischen Verhältnisse des Grossherzogtums Baden, Christian Theodor Groos, Karlsruhe, 1120 pp., 1846.

Wimmenauer, W., Liehl, E., and Schreiner, A.: Geologische Karte von Baden-Württemberg 1:25 000. Blatt 8114 Feldberg, Landesvermessungsamt Baden-Württemberg, Stuttgart, 1990.

Ziegler, P. A.: European Cenozoic rift system, Tectonophysics, 208, 91–111, https://doi.org/10.1016/0040-1951(92)90338-7, 1992.

Zweck, C., Zreda, M., and Desilets, D.: Snow shielding factors for cosmogenic nuclide dating inferred from Monte Carlo neutron transport simulations, Earth Planet. Sc. Lett., 379, 64–71, https://doi.org/10.1016/j.epsl.2013.07.023, 2013.